High particulate organic carbon export during the decline of a vast diatom bloom in the Atlantic sector of the Southern Ocean

Montserrat Roca-Martí [a], Viena Puigcorbé [a], Morten H. Iversen [b,c,d], Michiel Rutgers van der Loeff [b], Christine Klaas [b], Wee Cheah [b,e], Astrid Bracher [b,f], Pere Masqué [a,g,h]

Affiliation:

[a] Institut de Ciència i Tecnologia Ambientals & Departament de Física, Universitat Autònoma de Barcelona, 08193 Bellaterra, Spain
[b] Alfred Wegener Institute for Polar and Marine Research, 27570 Bremerhaven, Germany
[c] Faculty of Geosciences and MARUM, University of Bremen, 28359 Bremen, Germany
[d] Helmholtz Young Investigator Group SEAPUMP, Alfred Wegener Institute for Polar and Marine Research, 27570 Bremerhaven, Germany
[e] Research Center for Environmental Changes, Academia Sinica, Taipei 115, Taiwan
[f] Institute of Environmental Physics, University of Bremen, 28359 Bremen, Germany
[g] Oceans Institute and School of Physics, The University of Western Australia, Crawley WA 6009, Australia
[h] School of Natural Sciences and Centre for Marine Ecosystems Research, Edith Cowan University, Joondalup WA 6027, Australia

Abstract

Carbon fixation by phytoplankton plays a key role in the uptake of atmospheric CO_2 in the Southern Ocean. Yet, it still remains unclear how efficiently the particulate organic carbon (POC) is exported and transferred from ocean surface waters to depth during phytoplankton blooms. In addition, little is known about the processes that control the flux attenuation within the upper twilight zone. Here, we present results of downward POC and particulate organic nitrogen fluxes during the decline of a vast diatom bloom in the Atlantic sector of the Southern Ocean in summer 2012. We used thorium-234 (^{234}Th) as a particle tracer in combination with drifting sediment traps (ST). Their simultaneous use evidenced a sustained high export rate of ^{234}Th at 100 m depth in the weeks prior to and during the sampling period. The entire study area, of

approximately 8000 km^2, showed similar vertical export fluxes in spite of the heterogeneity in phytoplankton standing stocks and productivity, indicating a decoupling between production and export. The POC fluxes at 100 m were high, averaging 26 ± 15 mmol C m^{-2} d^{-1}, although the strength of the biological pump was generally low. Only <20% of the daily primary production reached 100 m, presumably due to an active recycling of carbon and nutrients. Pigment analyses indicated that direct sinking of diatoms likely caused the high POC transfer efficiencies (~60%) observed between 100 and 300 m, although faecal pellets and transport of POC linked to zooplankton vertical migration might have also contributed to downward fluxes.

1. Introduction

The Southern Ocean is an important sink for atmospheric CO_2 accounting for about 15-20% of the global oceanic uptake (Gruber et al., 2009; Takahashi et al., 2002), with a significant contribution from phytoplankton that fix CO_2 to organic carbon (Hauck et al., 2013). However, the strength and efficiency of the biological pump (i.e. export efficiency and transfer efficiency, respectively), as well as their controlling factors are poorly understood, especially during phytoplankton blooms (Buesseler and Boyd, 2009).

The export efficiency (i.e. the fraction of production that is exported from the upper ocean, usually taken as the base of the euphotic zone or 100 m) is low in much of the global ocean (<5-10%), but it is typically about 50% for blooms at high latitudes (Buesseler, 1998). However, previous studies in the Southern Ocean have reported lower export efficiencies during high-productive events (Jacquet et al., 2011; Planchon et al., 2015; Rutgers van der Loeff et al., 1997; Savoye et al., 2008). Furthermore, iron-fertilised blooms in the Southern Ocean show high variability in the fraction of

55 production being exported from the ocean surface. As an example, during SOFeX-South
56 (66ºS) the export efficiency was low (<10%, Buesseler et al., 2005), while during
57 EIFEX it was approximately 60%, indicating a very strong biological pump (Smetacek
58 et al., 2012). A number of factors may explain the differences observed in export
59 efficiencies, including phytoplankton community composition and study time frame.
60 Diatoms are key exporters of carbon from the ocean surface to deep waters and
61 sediments, and hence play an essential role in reducing the CO_2 content in the
62 atmosphere (Smetacek, 1999). Previous studies have shown that very low macronutrient
63 concentrations, specifically of silicic acid, prevent the development of diatom blooms in
64 benefit of flagellates, resulting in low particulate organic carbon (POC) export fluxes
65 from the ocean surface (Jacquet et al, 2011; Martin et al., 2013). Further, diatoms in the
66 Southern Ocean contribute differently to POC export according to their life cycle
67 strategy in which the degree of silicification is relevant (Assmy et al., 2013; Quéguiner,
68 2013). Moreover, since export lags production, the time scale of the studies may often
69 be too short to quantitively estimate the strength of the biological pump during bloom
70 events (Buesseler et al., 2004; Charette and Buesseler, 2000).

71 The transfer efficiency (i.e. the fraction of shallow export that is transferred to
72 depth) indicates the attenuation of the flux that takes place within a certain depth range.
73 While it is known that the attenuation of POC fluxes is sharpest in the upper twilight
74 zone, i.e. 100-300 m below the euphotic zone depth, our understanding of the processes
75 affecting sinking particles throughout this layer is still poor (Buesseler and Boyd, 2009).
76 The vertical flux of organic matter throughout the water column is dominated by large
77 particles such as marine snow and faecal pellets (Ebersbach et al., 2011; Fowler and
78 Knauer, 1986; Laurenceau-Cornec et al., 2015) that can be attenuated to a large extent
79 by zooplankton and microbial degradation (Giering et al., 2014; Iversen et al., 2010;

Kiørbe, 2000; Smith et al., 1992). However, packaging of slowly sinking phytoplankton cells into large faecal pellets may play a key role in increasing the export and transfer efficiencies in the Southern Ocean (Cavan et al., 2015; Le Moigne et al., 2014). Mineral ballasting also appears to alter the efficiency by which POC is transported to depth (e.g. Iversen and Robert, 2015; Klaas and Archer, 2002).

Thorium-234 (^{234}Th, half-life = 24.1 d) is widely used as a particle tracer, mainly of POC, since it is particle reactive and its half-life allows studying events occurring over short time scales, ranging from days to weeks, such as phytoplankton blooms (e.g. Buesseler et al., 1992; Rutgers van der Loeff et al., 1997). A deficit of ^{234}Th with respect to its parent ^{238}U is typically found in the upper ocean. Once the ^{234}Th downward flux at a specific depth is quantified, this flux can be converted to POC and particulate organic nitrogen (PON) fluxes by determining the POC/^{234}Th and PON/^{234}Th ratios, respectively, in sinking particles (Buesseler et al., 2006; Cochran and Masqué, 2003).

This study focuses on the decline of a vast diatom bloom that occurred in the Antarctic Circumpolar Current (ACC) region of the Southern Ocean (around 51ºS 13ºW) during the late austral summer in 2012. Our objectives were to evaluate the export efficiency and transfer efficiency of POC between 100 and 300 m, as well as identify the main mechanisms that had an influence on particle fluxes. Particle fluxes were quantified by means of two different techniques, as highly recommended given the uncertainties associated with each collection method (e.g. Puigcorbé et al., 2015; Turner, 2015). We used the disequilibrium between the natural radionuclides ^{234}Th and ^{238}U to determine the export fluxes of POC and PON in parallel with the use of surface-tethered drifting sediment traps. Export fluxes were related to the evolution of

chlorophyll *a* (Chl-a) and POC concentrations in the water column, as well as to pigments in sinking particles, following the decline of the bloom during three weeks. Net primary production (NPP) measured during the same cruise (Hoppe et al., this issue) was used to assess the export efficiency.

2. Methods

2.1. Study area

Samples were collected from 29 January to 17 February 2012 during the ANT-XXVIII/3 expedition in the Atlantic sector of the Southern Ocean (7 January-11 March, 2012; R/V Polarstern; Wolf-Gladrow, 2013). The sampling was carried out to study a massive bloom with high spatial and temporal resolution over an area of about 8000 km^2 located between the Antarctic Polar Front (APF) and the Southern Polar Front (SPF; Leach et al., and Strass et al., this issue). Time-series measurements of ^{234}Th, POC, PON, Chl-a, other pigments and NPP were carried out at a station located in the centre of the study area at 51.21ºS 12.67ºW (hereafter "central station", indicated by a 'C' in front of the station number). The location and sampling dates of the stations sampled for ^{234}Th, POC and PON fluxes are given in Figure 1 and Table 1.

2.2. Total ^{234}Th and ^{238}U

Total ^{234}Th activities were determined from 4 L seawater samples obtained from Niskin bottles attached to a CTD rosette. Samples were collected from 11-13 depths down to 500-750 m at 14 stations, with the highest resolution in the upper 200 m of the water column. Three seawater profiles were taken at the central station on 3, 12 and 17 February (C91, C128, C140, respectively). In addition, replicates of deep samples (2500 m) were collected for calibration purposes (Rutgers van der Loeff et al., 2006). The

samples were processed according to the MnO_2 co-precipitation technique (Buesseler et al., 2001b), using ^{230}Th as a chemical yield tracer (Pike et al., 2005). The precipitates were filtered through QMA quartz fibre filters, dried overnight at 50ºC and prepared for beta counting. The counting was done on board using low background beta counters (Risø National Laboratories, Denmark). Samples were re-measured after 10 months to quantify the background counts. All filters were processed to determine ^{230}Th by inductively coupled plasma mass spectrometry (ICP-MS) using ^{229}Th as an internal standard. Briefly, filters were spiked with ^{229}Th and precipitates were dissolved in 10 mL of 8M HNO_3/10% H_2O_2 solution. Samples were sonicated for 30 minutes before allowing them to rest for at least 6 hours. Prior to the ICP-MS analyses the samples were filtered through Acrodisc 0.2 μm syringe filters and reconstructed with 2.5% HNO_3/0.01% HF. The average chemical recovery of the analytical process was 94 ± 4% (n = 173), and the uncertainty of the $^{230}Th/^{229}Th$ ratios averaged 1.5 ± 0.6% (n = 173). The activity of ^{238}U was derived from salinity using the relationship given by Owens et al. (2011). The ^{234}Th activity uncertainties were calculated by propagating uncertainties associated with counting, detector background and calibration, ICP-MS measurements and ^{238}U activities, and were always <10% (average: 8.9 ± 0.3%, n = 173). All data of total ^{234}Th and ^{238}U activities are available at http://dx.doi.org/10.1594/PANGAEA.848823.

2.3. ^{234}Th, POC and PON in particles

Sinking particles were collected using surface-tethered sediment traps deployed for 1 to 3 days (Table 2). The sediment traps (ST) were attached to a drifting array with a surface buoy equipped with a GPS satellite transmitter, two surface floats and 12 buoyancy balls acting as wave breakers in order to reduce the hydrodynamic stress on

traps. The ST array was equipped with two sets of four gimbal mounted collection cylinders positioned at nominal depths of 100-120 m and 300-320 m, respectively. At each depth, three cylinders were filled with an unpoisoned brine solution for biogeochemical analyses and one cylinder with a viscous gel to preserve sinking particles in their original shape. This type of array was deployed a total of 11 times, including 7 deployments at the central station (C91, C98, C99, C114, C128, C136, C140) between 3 and 17 February. One of the cylinders for biogeochemical analyses was used after picking off swimmers under a binocular microscope: i) one half was filtered through a pre-combusted QMA filter to analyse ^{234}Th, POC and PON on the same filter as recommended by Buesseler et al. (2006); ii) the other half split was filtered using a pre-combusted GF/F filter to analyse POC and PON. The total POC and PON fluxes collected with the ST were determined as the average of the fluxes obtained from samples i) and ii). Additionally, four Challenger *in-situ* pumps (ISP) were deployed at 100, 150, 300 and 400 m at two stations (C91 and 139) to collect particles using 53-µm pore size nylon mesh screens (Table 2). Particles were subsequently rinsed with filtered seawater and re-filtered through a pre-combusted QMA filter to analyse ^{234}Th, POC and PON after removing swimmers from the filters. The activity of ^{234}Th in particles was first measured on board and re-measured at the home laboratory 10 months later as described for the water samples. POC and PON were determined with an EuroVector Elemental Analyser, pre-treating the filters with diluted HCl (Knap et al., 1996). The samples were corrected for POC and PON blanks (1.38 and 0.20 µmol, respectively), which on average represented about 2% of the POC and PON measurements.

2.4. Pigments in sediment traps

One fifth of a ST cylinder dedicated to biogeochemical analyses was used to analyse pigments after picking off swimmers. Diluted ST samples were filtered through GF/F filters, under low-vacuum pressure (below 20 kPa). Filtered samples were then immediately shock-frozen in liquid nitrogen and stored at -80°C until further analyses by high performance liquid chromatography (HPLC) at the Alfred-Wegener-Institute in Bremerhaven, Germany. Pigments from ST samples were analysed based on the HPLC method of Barlow et al. (1997) as detailed in Cheah et al. (this issue). The samples were measured using a Waters 600 (Waters, USA) controller combined with a Waters 2998 photodiode array detector, and a Water 717plus auto sampler. 100 µL of canthaxanthin was added to each sample as internal standard. Pigments were identified and quantified using the EMPOWER software provided by Waters. Three pigment-based phytoplankton size classes (micro-, nano-, and picophytoplankton) were estimated following the method of Uitz et al. (2009), which has been tested for the Southern Ocean waters. Microphytoplankton corresponded to phytoplankton with size >20 µm, nanophytoplankton between 2-20 µm, and picophytoplankton between 0.2-2 µm.

2.5. Chl-a and POC in the water column

Seawater samples for Chl-a (Chl-a_{SW}) and POC determination were obtained from Niskin bottles attached to the CTD rosette from 5 to 6 depths in the upper 100 m at 33 stations. For Chl-a_{SW} analysis, samples were filtered onto GF/F filters at pressure below 20 kPa. Filters were immediately transferred to centrifuge tubes with 10 ml 90% acetone and 1 cm^3 of glass beads. The tubes were sealed and stored at -20°C for at least 30 min. Chl-a was extracted by placing the centrifuge tubes in a grinder for 3 minutes followed by centrifugation at 0°C. The supernatant was poured in quartz tubes and measured for Chl-a content in a Turner 10-AU fluorometer. The fluorometer was

calibrated at the beginning and at the end of the expedition. Chl-a content was calculated using the equation given in Knap et al. (1996) using average parameter values from both calibrations. For POC analysis, samples were filtered onto pre-combusted GF/F filters at pressure not exceeding 20 kPa. Filters were immediately transferred to pre-combusted glass petri dishes and dried overnight at 50°C. Dried filters were stored at -20°C until analysis at the home laboratory using an EuroVector Elemental Analyser. The samples were corrected for POC blanks and the uncertainty of the POC measurements was 1.9% based on three reference standards.

2.6. Satellite Chl-a concentration

Satellite Chl-a concentrations were taken from the merged daily OC-CCI Chl-a data (ESACCI-OC-L3S product, ~4 km, version-2, http://www.oceancolour.org) and averaged over the time period of the study sampling. The OC-CCI data product combines the Medium Resolution Imaging Spectrometer (MERIS) on the Envisat satellite, the Moderate Resolution Imaging Spectrometer (MODIS) on the Aqua satellite and the Sea-viewing Wide Field-of-view Sensor (SeaWiFS) on the OrbView-2 satellite to one Chl-a product. This data product improves coverage of satellite Chl-a data in polar regions by a factor of two to three as compared to using the products of one single sensor. More details on the processing steps can be found in the product user guide (OC-CCI, 2015).

3. Results

3.1. Study area

Detailed hydrographic information can be found in Strass et al. and Leach et al. (this issue). The study area was placed between the APF and the SPF within the ACC

and around a central station located at 51.21ºS 12.67ºW. The main water masses identified were: Winter Water (WW, minimum potential temperature, θ_{min} = 1.1-1.9ºC, 100-200 m), Upper Circumpolar Deep Water (UCDW, θ_{max} = 2.1-2.4ºC, 400-500 m) and Antarctic Bottom Water (AABW, θ_{min} ~-0.2ºC). The mixed layer depth (MLD) varied from 24 to 98 m (average: 67 ± 18 m, n = 73, Strass et al., this issue). At the central station the structure of the upper water column varied over time: i) the MLD ranged from ~75 to 100 m, and some profiles did not show a homogeneous surface layer; ii) the location of the WW θ_{min} fluctuated several tens of meters above and below 150 m; iii) many profiles showed temperature inversions below the θ_{min} depth and fluctuations of salinity and density within the depth range 200-300 m during the second half of the sampling period. Moreover, at the central station currents flowing to the NE were intensified over time with speeds averaging from 2 to 10 cm s^{-1} for the top 500 m (Strass et al., this issue).

Satellite-derived Chl-a concentrations during the sampling period were, on average, lower than 1.5 mg m^{-3} (Figure 1), whereas at the peak of the bloom, during the first half of January, the Chl-a concentrations were ~3 mg m^{-3} (Hoppe et al., this issue). The euphotic zone depth ranged between 36 and 66 m (average: 45 ± 7 m, n = 40, Cheah et al., this issue). Nutrient concentrations and deficits are described in Hoppe et al. (this issue). On average, macronutrient concentrations within the euphotic zone were ~21 mmol NO_3 m^{-3}, ~1.4 mmol PO_4 m^{-3} and ~6.6 mmol $Si(OH)_4$ m^{-3}. High iron concentrations that allowed the development of the massive bloom likely reached the study site via advection through the ACC (L.M. Laglera pers. comm.). Concentrations of dissolved iron (<0.2 μm) were on average 0.12 ± 0.03 nM within the top 100 m of the water column (Hoppe et al., this issue), suggesting that dissolved iron was already depleted by phytoplankton activity during our sampling.

3.2. ^{234}Th activity profiles and fluxes

The vertical profiles of ^{234}Th and ^{238}U activity in the water column are shown in Figure 2. Significant deficits of ^{234}Th with respect to ^{238}U were present in surface waters down to 100-170 m at all stations, with ^{234}Th/^{238}U ratios averaging 0.67 ± 0.11 throughout the upper 100 m. In most cases, the base of these deficits matched well with the base of the Primary Production Zone (PPZ, Figure 2), defined as the depth at which fluorescence reaches 10% of its maximum value (Owens, 2013). The PPZ extended, on average, down to 117 ± 12 m, and the NPP at 100 m (deepest depth for NPP determination) ranged from 0.09 to 0.44 mmol C m^{-3} d^{-1}, confirming that primary production was occurring at least until 100 m (C. Hoppe pers. comm.). Below the PPZ, significant excess of ^{234}Th (^{234}Th/^{238}U ratio >1.1) was detected at stations C91 and 106 at one single depth (500 m). Significant ^{234}Th deficits (^{234}Th/^{238}U ratio <0.9) below the PPZ were also found at single depths at stations 93, C128, 137 and 139 (150, 750, 500 and 400 m, respectively). The central station showed a larger ^{234}Th deficit along the top 100 m during the second and third visits (C128 and C140: $(90 \pm 6)\cdot10^3$ and $(86 \pm 6)\cdot10^3$ dpm m^{-2}, respectively) compared to the first sampling (C91: $(71 \pm 6)\cdot10^3$ dpm m^{-2}).

^{234}Th fluxes (F_{Th}, in dpm m^{-2} d^{-1}) are attributed to scavenging of ^{234}Th onto particles sinking out of surface waters. Here, we estimated these fluxes using two methods: i) from seawater samples ($F_{Th,SW}$), and ii) directly from sediment traps ($F_{Th,ST}$). The $F_{Th,SW}$ were calculated using a steady state (SS) model, neglecting advective and diffusive fluxes (Buesseler et al., 1992):

$$F_{Th} = \lambda_{Th}(A_U - A_{Th}) \quad (1)$$

where λ_{Th} is the decay constant of ^{234}Th (0.029 d^{-1}) and (A_U - A_{Th}) is the integrated ^{234}Th deficit in the upper water column (dpm m^{-2}). We obtained the integrated ^{234}Th deficit with rectangular integration for two different horizon depths (100 and 300 m), allowing comparison with the ^{234}Th fluxes obtained directly from ST (Table 3).

Additionally, since the central station was sampled several times and the activity of ^{234}Th may have changed over time as a consequence of the sinking of the phytoplankton bloom (e.g. Savoye et al., 2006), ^{234}Th fluxes were also calculated using a non-steady state (NSS) model at 100 and 300 m (Table 4). This model assumes that the same water masses are sampled at all visits and ignores advective and diffusive fluxes of ^{234}Th (Savoye et al., 2006):

$$F_{Th} = \lambda_{Th}\left[\frac{A_U(1-e^{-\lambda\Delta t})+A_{Th1}e^{-\lambda\Delta t}-A_{Th2}}{1-e^{-\lambda\Delta t}}\right] \quad (2)$$

where A_U is the activity of ^{238}U, Δt is the time interval between two visits of a single station and A_{Th1} and A_{Th2} are the activities of ^{234}Th at the first and second visits, respectively.

$F_{Th,SW}$ and $F_{Th,ST}$ estimates at 100 and 300 m are presented in Tables 3-4 and Figure 3. Though some traps were placed 20 m deeper than the seawater sampling, we will still use 100 and 300 m to refer to 100 or 120 m and 300 or 320 m, respectively.

The SS estimates of $F_{Th,SW}$ at 100 m were relatively homogeneous over the entire study area and not significantly different from those at the base of the ^{234}Th deficit (~120 m, Wilcoxon test, $p > 0.05$), ranging from 1960 ± 210 to 3100 ± 180 dpm m^{-2} d^{-1} (average: 2390 ± 340 dpm m^{-2} d^{-1}, n = 14). Fluxes at 300 m had greater uncertainties than those at 100 m, and ranged from 1490 ± 710 to 3870 ± 700 dpm m^{-2}

291 d^{-1} (average: 2650 ± 610 dpm m^{-2} d^{-1}, n = 14). The $F_{Th,SW}$ over the study area showed no
292 significant differences between 100 and 300 m (t-test, p >0.05) (Figure 3). Focusing on
293 the central station, $F_{Th,SW}$ increased from C91 to C128 at both 100 and 300 m depth,
294 reaching ~3000 and 4000 dpm m^{-2} d^{-1}, respectively. The $F_{Th,SW}$ at station C140 were not
295 significantly different from those at station C128 (Table 3). According to the NSS
296 model, the $F_{Th,SW}$ decreased substantially from C91-C128 to C128-C140, especially at
297 300 m (Table 4).

298 $F_{Th,ST}$ at 100 m ranged from 1050 ± 90 to 4000 ± 320 dpm m^{-2} d^{-1} (average: 1720
299 ± 890 dpm m^{-2} d^{-1}, n = 10) (Table 3). A flux reduction of about 40% between 100 to
300 300 m was found at most stations, except at C128 and C140, where no significant
301 differences were observed. At the central station, $F_{Th,ST}$ at 100 m were relatively
302 constant from C91 to C140, with an average of 1330 ± 170 dpm m^{-2} d^{-1} (n = 6). $F_{Th,ST}$ at
303 300 m were also similar during the entire sampling time, averaging 900 ± 200 dpm m^{-2}
304 d^{-1} (n = 6).

305 Globally, the ^{234}Th fluxes estimated using the SS approach and ST were
306 comparable at 100 m (Wilcoxon test, p >0.05, $F_{Th,SW}/F_{Th,ST}$ = 1.7 ± 0.9, n = 7), whereas
307 at 300 m the $F_{Th,SW}$ were higher than the $F_{Th,ST}$ estimates by an average factor of 2.6 ±
308 1.7 (n = 7).

309 *3.2.1. Impact of physical transport processes on the $F_{Th,SW}$ estimates*

310 The physical transport processes can be parameterised as (e.g. Savoye et al.,
311 2006):

312 $$V = \pm u\frac{\partial A_{Th}}{\partial x} \pm v\frac{\partial A_{Th}}{\partial y} \pm w\frac{\partial A_{Th}}{\partial z} \pm K_x\frac{\partial^2 A_{Th}}{\partial x^2} \pm K_y\frac{\partial^2 A_{Th}}{\partial y^2} \pm K_z\frac{\partial^2 A_{Th}}{\partial z^2} \quad (3)$$

where advective and diffusive components are included along the x, y and z directions. Velocities are denoted by u, v and w, $\frac{\partial A_{Th}}{\partial x}$, $\frac{\partial A_{Th}}{\partial y}$ and $\frac{\partial A_{Th}}{\partial z}$ are the ^{234}Th activity gradients and K_x, K_y and K_z are the diffusion coefficients. Vertical advection needs to be considered in areas of established upwelling, while horizontal advection should be taken into account in ocean margins, where this process likely plays a relevant role (Savoye et al., 2006). During our survey the vertical advection was presumably negligible, while horizontal advection was significant with mean currents of about 7 cm s^{-1} for the top 100 and 300 m (V. Strass pers. comm.). Buesseler et al. (1994) showed that advection is dominant over diffusion in the horizontal transport of ^{234}Th in open waters. Therefore, we focused our attention on the horizontal advection in order to have a first estimate of the importance of the physical transport in the present study or, in other words, to test the accuracy of our ^{234}Th export estimates. We addressed this issue considering: i) the mean u and v velocities over the area 50.67-51.67ºS and 11.92-13.50ºW for the top 100 and 300 m: u = 5.6 cm s^{-1}, v = 4.3 cm s^{-1} and u = 5.7 cm s^{-1}, v = 3.9 cm s^{-1}, respectively (V. Strass pers. comm.); ii) the ^{234}Th activity gradients for the top 100 and 300 m (excluding station 86): $\frac{\partial A_{Th}}{\partial x}$ = (6.3 ± 7.9)·10^{-2} dpm m^{-3}, $\frac{\partial A_{Th}}{\partial y}$ = (7.4 ± 6.1)·10^{-2} dpm m^{-3} and $\frac{\partial A_{Th}}{\partial x}$ = (2.4 ± 3.0)·10^{-1} dpm m^{-3}, $\frac{\partial A_{Th}}{\partial y}$ = (0.9 ± 2.2)·10^{-1} dpm m^{-3}, respectively. In this way, the negligence of horizontal advection would lead to an error on the $F_{Th,SW}$ estimates of 580 ± 440 dpm m^{-2} d^{-1} at 100 m and 1500 ± 1700 dpm m^{-2} d^{-1} at 300 m. Thus, the physical processes would have a smaller impact on the $F_{Th,SW}$ estimates at 100 m (~25%) than at 300 m (~50%) at the investigated stations due to the smaller spatial variability of ^{234}Th activities in the upper 100 m.

Additionally, we have tested the influence of vertical diffusivity on ^{234}Th export

using an intermediate K_z value of 10^{-4} m^2 s^{-1} at 100 m (Strass et al. and Leach et al., this issue), obtaining a maximum contribution of this process of 30-180 dpm m^{-2} d^{-1}. Thus, the contribution of the vertical diffusivity to the $F_{Th,SW}$ estimates at 100 m must have been very small, generally lower than the uncertainties associated with the estimates. It was not possible to reproduce this exercise at 300 m due to the low ^{234}Th resolution around that depth.

3.2.2. SS vs NSS models at the central station

At the central station we determined the ^{234}Th export with both SS and NSS models. However, changes in the upper water column properties occurred during the sampling period, especially evident when station C128 was occupied (see section 3.1 and Strass et al. this issue), indicating that different water masses with particular scavenging histories were likely sampled. Furthermore, we have quantified an appreciable impact of advection on the $F_{Th,SW}$ estimates, especially at 300 m (see section 3.2.1). This has led us to discard the use of the NSS approach since it can produce large errors when spatial variability is misinterpreted as temporal variability, improving ^{234}Th export estimates only if sampling is conducted in a Lagrangian framework (Resplandy et al., 2012). Additionally, the results obtained from the NSS model (Table 4) are not consistent with results from the ST, which tend to be more constant. Thus, we consider that the SS model gives the best estimate of ^{234}Th export in this study.

3.3. POC/^{234}Th and PON/^{234}Th ratios in particles

POC/^{234}Th and PON/^{234}Th (C/Th and N/Th) ratios in particles from ST (C/Th_{ST} and N/Th_{ST}) and in particles >53 μm collected using ISP (C/Th_{ISP} and N/Th_{ISP}), usually considered to be sinking particles (e.g. Buesseler et al., 2006), are presented in Table 5.

C/Th_{ST} and N/Th_{ST} ratios at 100 m averaged 14 ± 3 and 1.7 ± 0.4 μmol dpm^{-1} (n = 10), respectively, and were about 30% lower at 300 m depth (10 ± 3 and 1.1 ± 0.3 μmol dpm^{-1}, n = 9, respectively). C/Th_{ISP} and N/Th_{ISP} ratios also decreased with depth between 100-150 and 300-400 m, by about 60%. At the central station, C/Th_{ST} and N/Th_{ST} ratios at 100 m decreased by 30% from the beginning until the end of the study, but no significant change was observed at 300 m.

ST and ISP ratios (C/Th and N/Th) were in reasonable agreement (within a factor of 1.4), except at station 139 at 100 m depth, where the ISP ratios were about 3-4 times higher than the ST ratios. The molar C/N ratio was 8 ± 1 for ST ratios (n = 19) and 7 ± 1 for ISP ratios (n = 8).

3.4. POC and PON fluxes

We used three methods to estimate POC and PON fluxes (F_C and F_N, respectively) (Table 5): i) measured directly with the ST (ST method: $F_{C,ST}$ and $F_{N,ST}$), ii) combining the $F_{Th,SW}$ and the ST ratios (SWST method: $F_{C,SWST}$ and $F_{N,SWST}$), and iii) combining the $F_{Th,SW}$ and the ISP ratios (SWISP method: $F_{C,SWISP}$ and $F_{N,SWISP}$). For ii) and iii) we used the SS estimates of F_{Th} and the C/Th (or N/Th) ratios in sinking particles, as:

$$F_C = F_{Th}(C/Th) \quad (4)$$

The average $F_{C,ST}$ and $F_{N,ST}$ at 100 m were 19 ± 9 and 2 ± 1 mmol m^{-2} d^{-1} (n = 11), respectively, with maxima at station 87. $F_{C,ST}$ and $F_{N,ST}$ at 300 m averaged 9 ± 3 and 1.0 ± 0.3 mmol m^{-2} d^{-1} (n = 11), respectively, about 60% less than the fluxes at 100 m except at stations C128, C136 and C140. During the occupation of the central station,

381 $F_{C,ST}$ and $F_{N,ST}$ at 100 m decreased by 25% over the study period, while they increased
382 by 30% and 50%, respectively, at 300 m.

383 $F_{C,SWST}$ and $F_{N,SWST}$ at 100 m averaged 30 ± 10 and 4 ± 1 mmol m^{-2} d^{-1} (n = 7),
384 respectively. Fluxes at 300 m averaged 20 ± 10 and 2 ± 1 mmol m^{-2} d^{-1} (n = 6),
385 respectively, about 40% less than the fluxes at 100 m except at stations C128 and C140.
386 $F_{C,SWST}$ and $F_{N,SWST}$ estimates at the central station showed changes <5% with time at
387 100 m, whereas the fluxes at 300 m were more variable, with a maximum $F_{C,SWST}$ of 50
388 ± 10 mmol m^{-2} d^{-1} at C128.

389 The SWISP method was used at the two stations where ISP were deployed.
390 $F_{C,SWST}$ and $F_{N,SWST}$ at station 139 were higher than at C91 by a factor of about 2, at both
391 100-150 m and 300-400 m. Fluxes at 300 m were lower than those at 100 m by 40%
392 (C91) and 70% (139).

393 Overall, the F_C and F_N estimated by using SW samples ($F_{C,SWST,}$ $F_{N,SWST}$ and
394 $F_{C,SWISP,}$ $F_{N,SWISP}$) were greater than those measured with ST by a factor of 2.0 ± 1.0 and
395 2.3 ± 1.3 (n = 17), respectively, at 100 m, and 2.4 ± 1.0 and 2.5 ± 1.0 (n = 17),
396 respectively, at 300 m.

397 *3.5. Chl-a and POC in the water column*

398 The Chl-a_{SW} inventories down to 100 m were, in most instances, larger than 100
399 mg m^{-2} (Figure 4A), with highest inventories (>180 mg m^{-2}) at the SE quadrant of the
400 study site, while stations 87 and 139, located to the NW, presented the lowest values
401 (~50 mg m^{-2}). At the central station the Chl-a_{SW} inventories ranged from 130 to 200 mg
402 m^{-2}, decreasing by about 30% from the beginning until the end of sampling, with
403 fluctuations over time. The POC inventories down to 100 m ranged from $10 \cdot 10^3$ to

404 $26 \cdot 10^3$ mg m^{-2}, showing a strong positive correlation with Chl-a_{SW} ($p < 0.001$; Pearson
405 correlation coefficient, $r = 0.84$; $n = 20$; Figure 4A).

406 *3.6. Pigments and POC in sediment traps*

407 In contrast to the water column, there was no significant correlation between the
408 fluxes of Chl-a measured with ST (Chl-a_{ST}) and $F_{C,ST}$, neither at 100 m ($p > 0.05$;
409 Spearman correlation coefficient, $\rho = -0.03$; $n = 11$) nor 300 m ($p > 0.05$, $\rho = 0.26$, $n =$
410 11, Figure 4B). Both Chl-a_{ST} fluxes and $F_{C,ST}$ decreased with depth (except Chl-a_{ST} flux
411 at station C114), although this decrease was stronger for POC at most stations (Figure 5,
412 Table 5).

413 Maximum Chl-a_{ST} flux was recorded at station C98 (0.79 mg m^{-2} d^{-1} at 100 m),
414 whereas minimum Chl-a_{ST} flux was observed at station 86 (0.11 mg m^{-2} d^{-1} at 300 m).
415 Fluxes of total pheopigments (TPheo, i.e. sum of pheophytin-a, pyropheophytin-a,
416 pheophorbide-a, and pyropheophorbide-a pigments) were generally higher at 100 m
417 than at 300 m except at stations C91 and C114 (Figure 5A). Maximum TPheo fluxes
418 were recorded at station 87 (2.67 and 1.27 mg m^{-2} d^{-1} at 100 and 300 m, respectively).
419 Ratios of TPheo/Chl-a_{ST} were generally higher at 100 m than at 300 m except at station
420 C91. TPheo/Chl-a_{ST} ratios above 1 were recorded at most of the investigated stations
421 except at 137, 139, C98, C136 and C140 (Figure 5A). Among the marker pigments,
422 fluxes of fucoxanthin were much higher than other pigments (Figure 5B) and the
423 phytoplankton size classification showed that more than 80% of the phytoplankton were
424 microphytoplankton (Figure 5C).

425 *4. Discussion*

426 *4.1. ^{234}Th fluxes*

427 *4.1.1. Seawater approach vs sediment traps*

428 In this study, the ^{234}Th fluxes were estimated using the seawater approach and
429 sediment traps. The SW approach integrates about 5 weeks before sampling (^{234}Th
430 mean life = 35 days), while ST provide information at the sampling time. In general, as
431 shown in section 3.2, the ^{234}Th fluxes based on these techniques were not significantly
432 different at 100 m. This agreement indicates a sustained export rate in the weeks prior to
433 and during the sampling period, suggesting export fluxes at steady state.

434 At 300 m the $F_{Th,ST}$ were about 3 times lower than the $F_{Th,SW}$. A review by
435 Buesseler et al. (2007) suggested that ^{234}Th-bearing particles were under-trapped by a
436 factor of about 2 and suggested some processes that could be sources of trap error, such
437 as under-collection of slow settling particles by hydrodynamic bias, particle
438 solubilisation within the trap before sample processing, and "swimmer" related
439 artefacts. Haskell et al. (2013) reported that ST collected about ≤20% of the $F_{Th,SW}$ in
440 two consecutive years and proposed that the main cause of this mismatch was the
441 under-trapping of small, ^{234}Th-enriched slow sinking particles. Additionally, the active
442 transport of surface-derived particles to hundreds of meters down via zooplankton
443 migration (e.g. Angel, 1989) is another factor that may lead to underestimation of the
444 particle export based on ST. Here, we tried to minimise the sources of error by using
445 two surface floats and 12 buoyancy balls as wave breakers, while the cylinders of the
446 ST were gimbal mounted. In addition, samples were processed within 24 h after
447 collection to decrease the impact of solubilisation and zooplankton swimmers on
448 material, which were picked under a binocular microscope.

449 Buesseler et al. (2007) also suggested that the mismatch between the SW
450 approach and ST could be related to the use of inaccurate assumptions in the ^{234}Th

451 model. The exclusion of physical processes in our study could introduce a significant
452 error on the $F_{Th,SW}$ estimates at 300 m (~50%, see section 3.2.1). Besides, in a late stage
453 of a bloom, the SS assumption may lead to an overestimation of the $F_{Th,SW}$ if higher
454 export occurred before sampling (within the ^{234}Th time scale). However, similar $F_{Th,SW}$
455 were found over the entire study area at both 100 and 300 m (Figure 3), irrespectively of
456 phytoplankton biomass (see section 3.5). This indicates that ^{234}Th fluxes probably did
457 not change significantly during the weeks before our arrival and, therefore, the SS
458 model gives reasonable estimates of ^{234}Th export flux.

459 *4.1.2. Results and comparison with other studies*

460 On average, ^{234}Th fluxes at 100 and 300 m were 2100 ± 700 and 2000 ± 1000
461 dpm m^{-2} d^{-1}, respectively. Hence, the fluxes were high and quite similar over the entire
462 study area, despite the differences observed in Chl-a_{SW} inventories (see section 3.5) and
463 production rates (Hoppe et al., this issue). However, satellite images show widespread
464 high Chl-a concentrations in January 2012 (data not shown). Thus, stations with low
465 phytoplankton biomass and production rates (e.g. stations 139 and C136) but high F_{Th}
466 evidenced a temporal decoupling between production and export. Buesseler et al. (2003,
467 2001a), Rutgers van der Loeff et al. (2011) and Henson et al. (2015) showed that export
468 lags production by up to 1-2 months in the Southern Ocean, which is a time frame
469 compatible with the present study.

470 Our F_{Th} estimates at 100 m are within the range of values for blooms during
471 their peak and/or decline occurring in the Southern Ocean, either in land remote areas
472 (Rutgers van der Loeff et al., 1997) or near islands (Morris et al., 2007; Savoye et al.,
473 2008). In contrast, our estimates are higher than the F_{Th} of ≤1000 dpm m^{-2} d^{-1} reported
474 during the onset of a bloom by Planchon et al. (2015), and during the artificial iron

475 fertilisation experiments SOIREE (Charette and Buesseler, 2000), EisenEx (Rutgers van
476 der Loeff and Vöge, 2001) and LOHAFEX (Martin et al., 2013). However, the SOFeX-
477 South experiment revealed an increase of particle fluxes after fertilisation, which
478 resulted in F_{Th} of ~1800 dpm m^{-2} d^{-1} at the MLD (Buesseler et al., 2005, 2004). The
479 variability within the plankton community structure and different sampling time
480 strategies among these experiments most likely played a crucial role in the variety of
481 results obtained (Boyd et al., 2007; Buesseler et al., 2004).

482 A release of ^{234}Th from sinking particles, either via remineralisation or
483 disaggregation, was evidenced by a 40% decrease of the $F_{Th,ST}$ between 100 and 300 m
484 at the majority of the stations. However, the seawater approach did not show excesses
485 of ^{234}Th in the depth range 100-300 m at any station. As a result, ^{234}Th flux attenuation
486 from 100 to 300 m estimated using the two methods was different at 3 out of 7 stations,
487 taking into account the large uncertainties of the $F_{Th,SW}$ estimates at 300 m (16-48%,
488 Table 3). The potential impact of advection on the $F_{Th,SW}$ estimates at 300 m (see
489 section 3.2.1) together with a low resolution of the seawater sampling between 100-300
490 m (2-3 samples) likely explain most of the disagreement between the ST and SW
491 approaches on this issue. Remineralisation and/or particle break-up was also indicated
492 in previous studies in the Southern Ocean (Buesseler et al., 2005; Planchon et al., 2013;
493 Rutgers van der Loeff et al., 2011; Savoye et al., 2004; Usbeck et al., 2002). In our
494 study, $F_{Th,ST}$ were attenuated between 100 and 300 m at the first 4 visits of the central
495 station, but not at stations C128 and C140 (Table 3), indicating that attenuation of $F_{Th,ST}$
496 in this depth range became negligible at the end of the sampling period. This
497 observation is similar to one of the major findings of the SOFeX-South experiment: the
498 attenuation of F_{Th} with depth disappeared as the bloom progressed (Buesseler et al.,
499 2005). This was attributed to changes in the nature of the sinking particles (less labile or

more rapidly sinking) and/or less efficient biological and physical processes responsible for particle break-up and consumption below the bloom.

4.2. POC/^{234}Th and PON/^{234}Th ratios in particles

C/Th and N/Th ratios were >10 μmol C dpm^{-1} (average: 15 ± 5 μmol C dpm^{-1}) and >1 μmol N dpm^{-1} (average: 2 ± 1 μmol N dpm^{-1}), respectively, in all samples collected either with ST or ISP (>53 μm) at 100 m. Overall, these values were higher than those reported by most studies conducted in the Southern Ocean (Buesseler et al., 2005, 2001a; Coppola et al., 2005; Jacquet et al., 2011; Martin et al., 2013; Morris et al., 2007; Planchon et al., 2013; Rutgers van der Loeff et al., 2011, 1997; Savoye et al., 2008), but similar to others (Cochran et al., 2000; Puigcorbé et al., this issue; Rutgers van der Loeff et al., 2002; Smetacek et al., 2012). Multiple factors may have played a role in shaping the C/Th and N/Th ratios, such as particle source, sinking velocity, Th speciation and remineralisation of C, N and ^{234}Th associated with sinking particles (Buesseler et al., 2006). Buesseler (1998) and Buesseler et al. (2006) hypothesised that high C/Th ratios encountered in productive regimes and high latitude areas may be related to the dominance of sinking of large cells, such as diatoms. This was explained by the fact that diatoms have a high volume relative to surface area (V:SA), and hence high C/Th ratios because C varies as a function of volume, whereas Th adsorption varies as a function of surface area. In our study, the dominance of fucoxanthin, a marker pigment for diatoms, and microphytoplankton in trap material (Figure 5B,C) revealed that diatoms were the major phytoplankton group contributing to vertical fluxes. Additionally, according to microscopic analyses (C. Klaas pers. comm.), the needle-shaped *Pseudo-nitzschia lineola* and the large centric diatom *Dactyliosolen antarcticus* dominated the bloom, with significant contributions from *Fragilariopsis*

524 *kerguelensis* as well as other *Pseudo-nitzschia*, *Rhizosolenia* and *Chaetoceros* species.
525 Thus, diatoms with a high V:SA, including *Dactyliosolen antarcticus* and *Chaetoceros*
526 spp. played a relevant role in the bloom, which could be responsible for the high ratios
527 observed.

528 C/Th and N/Th ratios at 300 m were, on average, about 30% lower than at 100
529 m. The reduction of C/Th ratios with depth is commonly observed (Buesseler et al.,
530 2006). It is likely due to the production of ^{234}Th in the entire water column leading to
531 additional adsorption of ^{234}Th onto particles at depth, which compensates its decay, and
532 a preferential remineralisation of POC with respect to ^{234}Th (Rutgers van der Loeff et
533 al., 2002). The same reasons would apply for PON.

534 The C/N ratios averaged 8 ± 1 and 7 ± 1 for ST and ISP samples, respectively,
535 and were within the range of values previously reported during bloom events (Martin et
536 al., 2013; Morris et al., 2007; Savoye et al., 2008), with a diverse composition of the
537 dominant particle type (diatoms: Salter et al., 2007; faecal material: Ebersbach and
538 Trull, 2008, and Ebersbach et al., 2014).

539 *4.3. POC and PON fluxes at 100 m*

540 POC and PON export fluxes at 100 m averaged 26 ± 15 mmol C m^{-2} d^{-1} (range:
541 11-67 mmol C m^{-2} d^{-1}) and 4 ± 2 mmol N m^{-2} d^{-1} (range: 1.6-12 mmol N m^{-2} d^{-1}, Table
542 5), respectively. Our F_C are high in relation to the average fluxes compiled by Le
543 Moigne et al. (2013) and Maiti et al. (2013). Le Moigne et al. (2013) reported an
544 average F_C of 9 ± 13 mmol C m^{-2} d^{-1} (n = 726; range: <0-125 mmol C m^{-2} d^{-1}) for the
545 global ocean, and 13 ± 14 mmol C m^{-2} d^{-1} (n = 196; range: 0-91 mmol C m^{-2} d^{-1}) for the

546 Southern Ocean. Maiti et al. (2013) reported a range of F_C from 1 to 50 mmol C m^{-2} d^{-1}
547 for the Southern Ocean, averaging 11 ± 8 mmol C m^{-2} d^{-1} (n = 140).

548 Considering other natural blooms observed in the Southern Ocean, our estimates
549 of F_C are comparable to those reported in KEOPS (average: 23 ± 4 mmol C m^{-2} d^{-1},
550 Savoye et al., 2008), the JGOFS Southern Ocean expedition (range: 20-39 mmol C m^{-2}
551 d^{-1}, Rutgers van der Loeff et al., 1997), and the CROZEX project (average: 14 ± 4
552 mmol C m^{-2} d^{-1}, Morris et al., 2007). Our estimates of F_N are also similar to the results
553 from KEOPS and CROZEX (Morris et al., 2007; Savoye et al., 2008). In contrast, our
554 F_C are higher than those reported in KEOPS II (average: 7 ± 2 mmol C m^{-2} d^{-1},
555 Planchon et al., 2015) for a bloom during its growing stage. On the other hand, the F_C
556 determined during SOIREE (Charette and Buesseler, 2000), SOFeX-South (Buesseler et
557 al., 2005) and LOHAFEX (Martin et al., 2013) were clearly lower (average ≤8 mmol C
558 m^{-2} d^{-1}) than in this study. In the case of LOHAFEX, it was explained by silica
559 limitation that prevented diatom growth. The low F_C measured during SOIREE and
560 SOFeX-South were likely due to a limited sampling period. However, the artificially
561 induced bloom during EIFEX (Smetacek et al., 2012) led to an extraordinarily high F_C
562 (~80 mmol C m^{-2} d^{-1}) with a high export efficiency. Thus, the high export fluxes found
563 in our study were comparable with other studies of the later stages of natural and iron
564 fertilised blooms in the Southern Ocean that were not silica limited.

565 *4.4. Export efficiency*

566 The export efficiency is a useful parameter to illustrate the strength of the
567 biological pump, even though production and export operate at distinct time scales
568 (Buesseler and Boyd, 2009). It should also be noted the temporal mismatch between the
569 measurements of production and export: 24 h incubation for NPP (Hoppe et al., this

570 issue), 15-72 h deployment for ST and a several weeks of integration for the SW
571 approach. We assessed the export efficiency by dividing the F_C at 100 m, either from
572 the SW methods or ST, by the NPP integrated down to 100 m (Hoppe et al., this issue).

573 The export efficiency within the bloom averaged 23 ± 24% (range: 7-100%;
574 Table 6, Figure 6A), taking into account all the techniques used to estimate the export of
575 POC (ST, SWST, SWISP). The export efficiency was around 10% according to the ST,
576 which is common in the open ocean (Buesseler, 1998), whereas it was around 25%
577 considering the SWST method. Besides these differences, the export efficiency was
578 always ≤50% for the ST and SWST methods, contrasting with export efficiencies >50%
579 reported during blooms at high latitudes, mostly characterized by large diatoms
580 (Buesseler, 1998; Smetacek et al., 2012) and a combination of *Phaeocystis* and diatoms
581 (Buesseler et al., 2003; Poulton et al., 2007). Other Southern Ocean studies (Buesseler
582 et al., 2005; Planchon et al., 2015) have also reported export efficiencies of ~10%
583 during not yet declining diatom blooms, where low POC export fluxes were measured
584 (7-8 mmol C m^{-2} d^{-1}). In contrast, during our study the bloom was declining, which lead
585 to high downward fluxes. We propose that this relatively low strength of the biological
586 pump was likely related to an active recycling of carbon and nutrients in surface waters.
587 Only for one station (139), which evidenced a temporal decoupling between production
588 and export (lowest Chl-a_{SW} inventories and NPP rates), the export efficiency was >30%
589 according to all techniques. Indeed, we found an inverse relationship between export
590 efficiency and NPP ($p < 0.05$; ST method: $\rho = -0.95$, $n = 8$; SWST method: $\rho = -0.89$, n
591 $= 6$) supporting recent observations (Cavan et al., 2015; Laurenceau-Cornec et al., 2015;
592 Maiti et al., 2013). This relationship could be explained by a combination of temporal
593 decoupling between primary production and export (Henson et al., 2015; Puigcorbé et

al., this issue), and other processes such as zooplankton grazing (Cavan et al., 2015), bacterial activity and recycling efficiency (Maiti et al., 2013).

4.5. Transfer efficiency

The upper 300 m of the water column is where intense biological and physical processes transform the size distribution of particles and thus modify the flux of particles to the mesopelagic layer (Guidi et al., 2009). To account for the change of the F_C magnitude within the upper twilight zone, we estimated the transfer efficiency by dividing the F_C at 300 m by those at 100 m.

The transfer efficiency averaged 59 ± 26% (range: 35->100%; Table 6, Figure 6B) with a general discrepancy among techniques <30%. Most of the transfer efficiencies were higher than the estimates presented by i) Schlitzer (2002): 40% for the same depth range using an inverse model based on observations of temperature, salinity and nutrient concentrations; and ii) Guidi et al. (2009): <42% when microphytoplankton dominated the phytoplankton community based on a world-ocean analysis. Guidi et al. (2009) showed that maximum values of F_C at 400 m were associated with a dominance of microphytoplankton in the euphotic zone, although the flux experienced a sharp decrease from 100 to 300 m with this community structure. In our study, the transfer efficiency at the central station was lower during the first 4 visits (C91-C114: 42 ± 6%) than during the last 3 (C128-C140: 70 ± 10%) according to the ST results (Table 6). This change coincided with a decrease of the TPheo/Chl-a_{ST} ratio in the trap material from the first group of stations to the second: from 2.5 ± 1.1 to 0.9 ± 0.8 at 100 m and from 3.5 ± 1.7 to 0.3 ± 0.2 at 300 m (Figure 5A). Pheopigments are degraded Chl-a products that are associated with grazing activity and phytoplankton senescence (Wright et al., 2010). Thus, this observation indicates that when the transfer efficiency was

618 higher, the organic material being exported was fresher. Indeed, there is a negative
619 relationship between TPheo/Chl-a_{ST} ratios at 100 m and the transfer efficiency of POC
620 from 100 to 300 m derived from ST ($p < 0.01$; $\rho = -0.77$, $n = 10$). This correlation
621 highlights the relevance of the particle composition sinking out from the ocean surface
622 in shaping the efficiency of the biological pump. Buesseler and Boyd (2009) pointed out
623 that very high transfer efficiencies are attributed to direct sinking of algae with low flux
624 attenuation. Here, more than 60% of the Chl-a_{ST} and fucoxanthin fluxes at 100 m
625 reached 300 m (Figure 5A,B), which highlights the contribution of diatoms to vertical
626 fluxes in the study area. In particular, the direct sinking of diatoms might be the main
627 explanation for the high transfer efficiencies at stations C136 and C140, since at these
628 locations the high fucoxanthin fluxes at 100 m (>0.4 mg m^{-2} d^{-1}) showed a decrease of
629 only ~10-20% at 300 m, and the TPheo/Chl-a_{ST} ratios were <1 (Figure 5A,B). Indeed, a
630 study by Cedhagen et al. (2014) from the same cruise showed that abyssal benthic
631 foraminifera at ~4000 m were feeding on fresh phytodetritus. This further indicates that
632 at least part of the phytoplankton at the surface waters were transported down to the
633 seabed.

634 The lack of relationship between Chl-a_{ST} and $F_{C,ST}$ at both 100 and 300 m depth
635 (Figure 4B), however, indicated that reprocessed material or dead phytoplankton also
636 contributed significantly to the export fluxes at most stations. The high fluxes of
637 pheopigments (>0.6 mg m^{-2} d^{-1}) together with TPheo/Chl-a_{ST} ratios >1 (Figure 5A) at
638 stations 87, C91, C99 and C114 at 100 and 300 m may be associated with grazing
639 activity and, hence, indicate the contribution of faecal pellets to sinking fluxes.
640 Preliminary results confirmed a significant abundance of faecal pellets in trap material
641 during our survey (Iversen and Klaas, 2013), although this should be validated by
642 quantitative analyses in the future. Specifically, at station C114 the TPheo, Chl-a_{ST} and

fucoxanthin fluxes increased from 100 to 300 m (Figure 5A,B), which may have been due to zooplankton consumption of diatoms in the euphotic zone and release of faecal pellets between 100 and 300 m. Therefore, production of faecal pellets and zooplankton vertical migration might have modulated the transfer efficiency in this study. Similar conclusions have been reached by Buesseler and Boyd (2009) and Cavan et al. (2015).

5. Conclusions

We measured downward fluxes of POC and PON during the decline of a vast diatom bloom in a land-remote area of the Atlantic sector of the Southern Ocean. Our main conclusions are:

1) The simultaneous use of sediment traps and the $^{234}Th/^{238}U$ proxy evidenced that ^{234}Th export rates at 100 m were high and constant in the weeks prior to and during the survey.
2) Stations distributed over an area of 8000 km^2 showed similar vertical export fluxes in spite of the heterogeneity in phytoplankton standing stocks and productivity, indicating a decoupling between production and export.
3) The diatom bloom led to high POC export fluxes at 100 m (26 ± 15 mmol C m^{-2} d^{-1}), although the export efficiencies were generally low (<20%) in comparison to other diatom blooms at high latitudes. An active recycling of carbon and nutrients in surface waters was likely the reason for the low export efficiencies.
4) In contrast to the low export efficiencies at 100 m depth, the transfer efficiency of POC between 100 and 300 m was high during the entire study period (~60%), partly driven by the sinking of fresh diatoms. Faecal pellets and the active transport of POC linked to zooplankton vertical migration may have also contributed significantly to vertical fluxes. If we are to understand the efficiency

667 of the biological pump in the Southern Ocean, these processes should be further
668 investigated in the future.

669 Acknowledgements

670 We are very grateful to the crew and scientific party of the R/V Polarstern ANT-XXVIII/3
671 expedition for their support at sea during more than two months. Thanks to the European Space
672 Agency (ESA) for OC-CCI data. We wish to acknowledge I. Stimac for her assistance with the
673 cruise preparation and ICPMS analyses, S. Wiegmann for her help with the HPLC analysis in
674 sediment trap samples, and M. Donnelly for his support deploying the *in-situ* pumps. The
675 authors acknowledge C. Hoppe, V.H. Strass, D. Wolf-Gladrow and M.A. Soppa for providing
676 valuable comments on earlier drafts. The manuscript was improved by comments from F.
677 Planchon and an anonymous reviewer. This project was partly supported by the Ministerio de
678 Ciencia e Innovación (CTM2011-14027-E, Spain) and the Generalitat de Catalunya to the
679 research group MERS (2014 SGR-1356). M.R-M. and V.P. acknowledge financial support
680 through PhD fellowships (AP2010-2510 and AP2009-4733, respectively) from the Spanish
681 government. Support for the research of P.M. was received through a Gledden Visiting
682 Fellowship awarded by the Institute of Advanced Studies at The University of Western
683 Australia. Funding to W.C. and to A.B. was supplied partly by the Helmholtz Innovation Fund
684 Phytooptics. M.H.I. was supported by the Helmholtz Association, the Alfred Wegener Institute
685 for Polar and Marine Research, HGF Young Investigator Group "SeaPump", and the DFG-
686 Research Center/Cluster of Excellence "The Ocean in the Earth System".

687 References

688 Angel, M. V, 1989. Does mesopelagic biology affect the vertical flux? In: Productivity
689 of the oceans: Present and past, Geological Journal. John Wiley and Sons, New
690 York. doi:10.1002/gj.3350260119

691

692 Assmy, P., Smetacek, V., Montresor, M., Klaas, C., Henjes, J., Strass, V.H., Arrieta,
693 J.M., Bathmann, U., Berg, G.M., Breitbarth, E., Cisewski, B., Friedrichs, L.,
694 Fuchs, N., Herndl, G.J., Jansen, S., Krägefsky, S., Latasa, M., Peeken, I., Röttgers,
695 R., Scharek, R., Schüller, S.E., Steigenberger, S., Webb, A., Wolf-Gladrow, D.,
696 2013. Thick-shelled, grazer-protected diatoms decouple ocean carbon and silicon
697 cycles in the iron-limited Antarctic Circumpolar Current. Proc. Natl. Acad. Sci. U.
698 S. A. 110, 20633–8. doi:10.1073/pnas.1309345110

699 Barlow, R.., Cummings, D.., Gibb, S.., 1997. Improved resolution of mono- and divinyl
700 chlorophylls a and b and zeaxanthin and lutein in phytoplankton extracts using
701 reverse phase C-8 HPLC. Mar. Ecol. Ser. 161, 303–307. doi:10.3354/meps161303

702 Boyd, P.W., Jickells, T., Law, C.S., Blain, S., Boyle, E.A., Buesseler, K.O., Coale,
703 K.H., Cullen, J.J., de Baar, H.J.W., Follows, M., Harvey, M., Lancelot, C.,
704 Levasseur, M., Owens, N.P.J., Pollard, R., Rivkin, R.B., Sarmiento, J.,
705 Schoemann, V., Smetacek, V., Takeda, S., Tsuda, A., Turner, S., Watson, A.J.,
706 2007. Mesoscale iron enrichment experiments 1993-2005: synthesis and future
707 directions. Science 315, 612–7. doi:10.1126/science.1131669

708 Buesseler, K.O., 1998. The decoupling of production and particulate export in the
709 surface ocean. Global Biogeochem. Cycles 12, 297–310. doi:10.1029/97GB03366

710 Buesseler, K.O., Andrews, J.E., Pike, S.M., Charette, M.A., 2004. The effects of iron
711 fertilization on carbon sequestration in the Southern Ocean. Science 304, 414–417.
712 doi:10.1126/science.1086895

713 Buesseler, K.O., Andrews, J.E., Pike, S.M., Charette, M.A., Goldson, L.E., Brzezinski,
714 M.A., Lance, V.P., 2005. Particle export during the Southern Ocean Iron
715 Experiment (SOFeX). Limnol. Oceanogr. 50, 311–327.
716 doi:10.4319/lo.2005.50.1.0311

717 Buesseler, K.O., Antia, A.N., Chen, M., Fowler, S.W., Gardner, W.D., Gustafsson, O.,
718 Harada, K., Michaels, A.F., Rutgers van der Loeff, M.M., Sarin, M., Steinberg,
719 D.K., Trull, T., 2007. An assessment of the use of sediment traps for estimating
720 upper ocean particle fluxes. J. Mar. Res. 65, 345–416.

721 Buesseler, K.O., Bacon, M.P., Cochran, J.K., Livingston, H.D., 1992. Carbon and
722 nitrogen export during the JGOFS North Atlantic Bloom experiment estimated
723 from 234Th: 238U disequilibria. Deep Sea Res. Part A. Oceanogr. Res. Pap. 39,
724 1115–1137. doi:10.1016/0198-0149(92)90060-7

725 Buesseler, K.O., Ball, L., Andrews, J., Cochran, J.K., Hirschberg, D.J., Bacon, M.P.,
726 Fleer, A., Brzezinski, M., 2001a. Upper ocean export of particulate organic carbon
727 and biogenic silica in the Southern Ocean along 170°W. Deep Sea Res. Part II
728 Top. Stud. Oceanogr. 48, 4275–4297. doi:10.1016/S0967-0645(01)00089-3

729 Buesseler, K.O., Barber, R.T., Dickson, M.L., Hiscock, M.R., Moore, J.K., Sambrotto,
730 R., 2003. The effect of marginal ice-edge dynamics on production and export in
731 the Southern Ocean along 170 degrees W. Deep. Res. Part II-Topical Stud.
732 Oceanogr. 50, 579 – 603. doi:10.1016/S0967-0645(02)00585-4

733 Buesseler, K.O., Benitez-Nelson, C., Rutgers van der Loeff, M.M., Andrews, J., Ball,
734 L., Crossin, G., Charette, M.A., 2001b. An intercomparison of small- and large-
735 volume techniques for thorium-234 in seawater. Mar. Chem. 74, 15–28.
736 doi:10.1016/S0304-4203(00)00092-X

737 Buesseler, K.O., Benitez-Nelson, C.R., Moran, S.B., Burd, A., Charette, M., Cochran,
738 J.K., Coppola, L., Fisher, N.S., Fowler, S.W., Gardner, W.D., Guo, L.D.,
739 Gustafsson, Ö., Lamborg, C., Masqué, P., Miquel, J.C., Passow, U., Santschi, P.H.,
740 Savoye, N., Stewart, G., Trull, T., 2006. An assessment of particulate organic
741 carbon to thorium-234 ratios in the ocean and their impact on the application of
742 234Th as a POC flux proxy. Mar. Chem. 100, 213–233.
743 doi:10.1016/j.marchem.2005.10.013

744 Buesseler, K.O., Boyd, P., 2009. Shedding light on processes that control particle export
745 and flux attenuation in the twilight zone of the open ocean. Limnol. Oceanogr. 54,
746 1210–1232. doi:10.4319/lo.2009.54.4.1210

747 Buesseler, K.O., Michaels, A.F., Siegel, D.A., Knap, A.H., 1994. A three dimensional
748 time-dependent approach to calibrating sediment trap fluxes. Global Biogeochem.
749 Cycles 8, 179–193. doi:10.1029/94GB00207

750 Cavan, E.L., Le Moigne, F.A.C., Poulton, A.J., Tarling, G.A., Ward, P., Daniels, C.J.,
751 Fragoso, G., Sanders, R., 2015. Attenuation of particulate organic carbon flux in
752 the Scotia Sea, Southern Ocean, is controlled by zooplankton fecal pellets.
753 Geophys. Res. Lett. 821–830. doi:10.1002/2014GL062744

754 Cedhagen, T., Cheah, W., Bracher, A., Lejzerowicz, F., 2014. Algal pigments in
755 Southern Ocean abyssal foraminiferans indicate pelagobenthic coupling. Deep.
756 Res. Part II 108, 27–32. doi:10.1016/j.dsr2.2014.07.017

757 Charette, M.A., Buesseler, K.O., 2000. Does iron fertilization lead to rapid carbon
758 export in the Southern Ocean? Geochemistry, Geophys. Geosystems 1, 1–7.
759 doi:10.1029/2000GC000069

760 Cheah, W., Soppa, M.A., Wiegmann, S., Ossebaar, S., Laglera, L.M., Strass, V.H.,
761 Santos-Echeandía, J., Hoppema, M., Wolf-Gladrow, D., Bracher, A., this issue.
762 Importance of deep-mixing and silicic acid in regulating phytoplankton biomass
763 and composition in the iron-limited Antarctic Polar Front region in summer. Deep
764 Sea Res. II.

765 Cochran, J.K., Buesseler, K.O., Bacon, M.P., Wang, H.W., Hirschberg, D.J., Ball, L.,
766 Andrews, J., Crossin, G., Fleer, A., 2000. Short-lived thorium isotopes (Th-234,
767 Th-228) as indicators of POC export and particle cycling in the Ross Sea, Southern
768 Ocean. Deep. Res. Part II-Topical Stud. Oceanogr. 47, 3451 – 3490.
769 doi:10.1016/S0967-0645(00)00075-8

770 Cochran, J.K., Masqué, P., 2003. Short-lived U/Th Series Radionuclides in the Ocean:
771 Tracers for Scavenging Rates, Export Fluxes and Particle Dynamics. Rev. Mineral.
772 Geochemistry 52, 461–492. doi:10.2113/0520461

773 Coppola, L., Roy-Barman, M., Mulsow, S., Povinec, P., Jeandel, C., 2005. Low
774 particulate organic carbon export in the frontal zone of the Southern Ocean (Indian
775 sector) revealed by 234Th. Deep Sea Res. Part I Oceanogr. Res. Pap. 52, 51–68.
776 doi:10.1016/j.dsr.2004.07.020

777 Ebersbach, F., Assmy, P., Martin, P., Schulz, I., Wolzenburg, S., Nöthig, E.-M., 2014.
778 Particle flux characterisation and sedimentation patterns of protistan plankton
779 during the iron fertilisation experiment LOHAFEX in the Southern Ocean. Deep
780 Sea Res. Part I Oceanogr. Res. Pap. 89, 94–103. doi:10.1016/j.dsr.2014.04.007

781 Ebersbach, F., Trull, T.W., 2008. Sinking particle properties from polyacrylamide gels
782 during the KErguelen Ocean and Plateau compared Study (KEOPS): Zooplankton
783 control of carbon export in an area of persistent natural iron inputs in the Southern
784 Ocean. Limnol. Oceanogr. 53, 212–224. doi:10.4319/lo.2008.53.1.0212

785 Ebersbach, F., Trull, T.W., Davies, D.M., Bray, S.G., 2011. Controls on mesopelagic
786 particle fluxes in the Sub-Antarctic and Polar Frontal Zones in the Southern Ocean
787 south of Australia in summer—Perspectives from free-drifting sediment traps.
788 Deep Sea Res. Part II Top. Stud. Oceanogr. 58, 2260–2276.
789 doi:10.1016/j.dsr2.2011.05.025

790 Fowler, S.W., Knauer, G.A., 1986. Role of large particles in the transport of elements
791 and organic compounds through the oceanic water column. Prog. Oceanogr. 16,
792 147–194. doi:10.1016/0079-6611(86)90032-7

793 Giering, S.L.C., Sanders, R., Lampitt, R.S., Anderson, T.R., Tamburini, C., Boutrif, M.,
794 Zubkov, M. V, Marsay, C.M., Henson, S.A., Saw, K., Cook, K., Mayor, D.J.,
795 2014. Reconciliation of the carbon budget in the ocean's twilight zone. Nature 507,
796 480–483. doi:10.1038/nature13123

797 Gruber, N., Gloor, M., Mikaloff Fletcher, S.E., Doney, S.C., Dutkiewicz, S., Follows,
798 M.J., Gerber, M., Jacobson, A.R., Joos, F., Lindsay, K., Menemenlis, D., Mouchet,
799 A., Müller, S.A., Sarmiento, J.L., Takahashi, T., 2009. Oceanic sources, sinks, and
800 transport of atmospheric CO2. Global Biogeochem. Cycles 23, 1–21.
801 doi:10.1029/2008GB003349

802 Guidi, L., Stemmann, L., Jackson, G.A., Ibanez, F., Claustre, H., Legendre, L., Picheral,
803 M., Gorsky, G., 2009. Effects of phytoplankton community on production, size and
804 export of large aggregates: A world-ocean analysis. Limnol. Oceanogr. 54, 1951–
805 1963. doi:10.4319/lo.2009.54.6.1951

806 Haskell, W.Z., Berelson, W.M., Hammond, D.E., Capone, D.G., 2013. Particle sinking
807 dynamics and POC fluxes in the Eastern Tropical South Pacific based on 234Th
808 budgets and sediment trap deployments. Deep. Res. Part I Oceanogr. Res. Pap. 81,
809 1–13. doi:10.1016/j.dsr.2013.07.001

810 Hauck, J., Völker, C., Wang, T., Hoppema, M., Losch, M., Wolf-Gladrow, D.A., 2013.
811 Seasonally different carbon flux changes in the Southern Ocean in response to the
812 southern annular mode. Global Biogeochem. Cycles 27, 1236–1245.
813 doi:10.1002/2013GB004600

814 Henson, S.A., Yool, A., Sanders, R., 2015. Variability in efficiency of particulate
815 organic carbon export: A model study. Global Biogeochem. Cycles 29, 33–45.
816 doi:10.1002/2014GB004965

817 Hoppe, C.J.., Klaas, C., Ossebaar, S., Soppa, M.A., Cheah, W., Laglera, L.M., Santos-
818 Echeandía, J., Rost, B., Wolf-Gladrow, D.A., Bracher, A., Hoppema, M., Strass,
819 V.H., Trimborn, S., this issue. Controls of primary production in two
820 phytoplankton blooms in the Antarctic Circumpolar Current. Deep Sea Res. II.

821 Iversen, M.H., Klaas, C., 2013. Controls on the vertical fluxes of the Southern Ocean,
822 in: The Expedition of the Research Vessel "Polarstern" to the Antarctic in 2012
823 (ANT-XXVIII/3). Bremerhaven, pp. 70–74.

824 Iversen, M.H., Nowald, N., Ploug, H., Jackson, G.A., Fischer, G., 2010. High resolution
825 profiles of vertical particulate organic matter export off Cape Blanc, Mauritania:
826 Degradation processes and ballasting effects. Deep Sea Res. Part I Oceanogr. Res.
827 Pap. 57, 771–784. doi:10.1016/j.dsr.2010.03.007

828 Iversen, M.H., Robert, M.L., 2015. Ballasting effects of smectite on aggregate
829 formation and export from a natural plankton community. Mar. Chem.
830 doi:10.1016/j.marchem.2015.04.009

831 Jacquet, S.H.., Lam, P.J., Trull, T., Dehairs, F., 2011. Carbon export production in the
832 subantarctic zone and polar front zone south of Tasmania. Deep Sea Res. Part II
833 Top. Stud. Oceanogr. 58, 2277–2292. doi:10.1016/j.dsr2.2011.05.035

834 Kiørbe, T., 2000. Colonization of marine snow aggregates by invertebrate zooplankton:
835 Abundance, scaling, and possible role. Limnol. Oceanogr. 45, 479–484.
836 doi:10.4319/lo.2000.45.2.0479

837 Klaas, C., Archer, D.E., 2002. Association of sinking organic matter with various types
838 of mineral ballast in the deep sea: Implications for the rain ratio. Global
839 Biogeochem. Cycles 16, 63–1–63–14. doi:10.1029/2001GB001765

840 Knap, A., Michaels, A., Close, A., Ducklow, H., Dickson, A., 1996. Protocols for the
841 Joint Global Ocean Flux Study (JGOFS) Core Measurements. JGOFS Report Nr.
842 19.

843 Lam, P.J., Bishop, J.K.B., 2007. High biomass, low export regimes in the Southern
844 Ocean. Deep Sea Res. Part II Top. Stud. Oceanogr. 54, 601–638.
845 doi:10.1016/j.dsr2.2007.01.013

846 Laurenceau-Cornec, E.C., Trull, T.W., Davies, D.M., Bray, S.G., Doran, J., Planchon,
847 F., Carlotti, F., Jouandet, M.-P., Cavagna, A.-J., Waite, A.M., Blain, S., 2015. The
848 relative importance of phytoplankton aggregates and zooplankton fecal pellets to
849 carbon export: insights from free-drifting sediment trap deployments in naturally
850 iron-fertilised waters near the Kerguelen Plateau. Biogeosciences 12, 1007–1027.
851 doi:10.5194/bg-12-1007-2015

Le Moigne, F.A.C., Henson, S.A., Sanders, R.J., Madsen, E., 2013. Global database of surface ocean particulate organic carbon export fluxes diagnosed from the ^{234}Th technique. Earth Syst. Sci. Data 5, 295–304. doi:10.5194/essd-5-295-2013

Le Moigne, F.A.C., Pabortsava, K., Marcinko, C.L.J., Martin, P., Sanders, R.J., 2014. Where is mineral ballast important for surface export of particulate organic carbon in the ocean? Geophys. Res. Lett. 1–9. doi:10.1002/2014GL061678

Leach, H., Strass, V.H., Prandke, H., this issue. Mixing and finescale structures in two mesoscale features of the Antarctic Circumpolar Current. Deep Sea Res. II.

Maiti, K., Charette, M.A., Buesseler, K.O., Kahru, M., 2013. An inverse relationship between production and export efficiency in the Southern Ocean. Geophys. Res. Lett. 40, 1557–1561. doi:10.1002/grl.50219

Martin, P., Rutgers van der Loeff, M.M.R., Cassar, N., Vandromme, P., D'Ovidio, F., Stemmann, L., Rengarajan, R., Soares, M., González, H.E., Ebersbach, F., Lampitt, R.S., Sanders, R., Barnett, B.A., Smetacek, V., Naqvi, S.W.A., 2013. Iron fertilization enhanced net community production but not downward particle flux during the Southern Ocean iron fertilization experiment LOHAFEX. Global Biogeochem. Cycles 27, 871–881. doi:10.1002/gbc.20077

Morris, P.J., Sanders, R., Turnewitsch, R., Thomalla, S., 2007. 234Th-derived particulate organic carbon export from an island-induced phytoplankton bloom in the Southern Ocean. Deep Sea Res. Part II Top. Stud. Oceanogr. 54, 2208–2232. doi:10.1016/j.dsr2.2007.06.002

OC-CCI, 2015. Ocean Color Climate Change Initiative Product User Guide Version 2. Ed. By M. Grant, T. Jackson, A. Chuprin, S. Sathyendranath, M. Zühlke, T. Storm, M. Boettcher, N. Fomferra, © Plymouth Marine Laboratory.

Owens, S.A., 2013. Advances in measurements of particle cycling and fluxes in the ocean. Massachusetts Institute of Technology and Woods Hole Oceanographic Institution, Woods Hole, MA. doi:10.1575/1912/5746

Owens, S.A., Buesseler, K.O., Sims, K.W.W., 2011. Re-evaluating the 238U-salinity relationship in seawater: Implications for the 238U–234Th disequilibrium method. Mar. Chem. 127, 31–39. doi:10.1016/j.marchem.2011.07.005

Pike, S., Buesseler, K., Andrews, J., Savoye, N., 2005. Quantification of 234Th recovery in small volume sea water samples by inductively coupled plasma-mass spectrometry. J. Radioanal. Nucl. Chem. 263, 355–360. doi:10.1007/s10967-005-0594-z

Planchon, F., Ballas, D., Cavagna, A.-J., Bowie, A.R., Davies, D., Trull, T., Laurenceau-Cornec, E.C., Van Der Merwe, P., Dehairs, F., 2015. Carbon export in the naturally iron-fertilized Kerguelen area of the Southern Ocean based on the 234Th approach. Biogeosciences 12, 3831–3848. doi:10.5194/bg-12-3831-2015

Planchon, F., Cavagna, A.-J., Cardinal, D., André, L., Dehairs, F., 2013. Late summer particulate organic carbon export and twilight zone remineralisation in the Atlantic sector of the Southern Ocean. Biogeosciences 10, 803–820. doi:10.5194/bg-10-803-2013

Poulton, A.J., Mark Moore, C., Seeyave, S., Lucas, M.I., Fielding, S., Ward, P., 2007. Phytoplankton community composition around the Crozet Plateau, with emphasis on diatoms and Phaeocystis. Deep Sea Res. Part II Top. Stud. Oceanogr. 54, 2085–2105. doi:10.1016/j.dsr2.2007.06.005

Puigcorbé, V., Benitez-Nelson, C.R., Masqué, P., Verdeny, E., White, A.E., Popp, B.N., Prahl, F.G., Lam, P.J., 2015. Small phytoplankton drive high summertime carbon and nutrient export in the Gulf of California and Eastern Tropical North Pacific. Global Biogeochem. Cycles 29, 1309–1332. doi:10.1002/2015GB005134

Puigcorbé, V., Roca-Martí, M., Masqué, P., Benitez-Nelson, C.R., Rutgers van der Loeff, M.M., Laglera, L.M., Bracher, A., Cheah, W., Strass, V.H., Hoppema, M., Santos-Echeandía, J., Klaas, C., this issue. Particulate organic carbon export across the Antarctic Circumpolar Current at 10ºE: Differences north and south of the Antarctic Polar Front. Deep Sea Res. II.

Quéguiner, B., 2013. Iron fertilization and the structure of planktonic communities in high nutrient regions of the Southern Ocean. Deep Sea Res. Part II Top. Stud. Oceanogr. 90, 43–54. doi:10.1016/j.dsr2.2012.07.024

Resplandy, L., Martin, A.P., Le Moigne, F., Martin, P., Aquilina, A., Mémery, L., Lévy, M., Sanders, R., 2012. How does dynamical spatial variability impact 234Th-derived estimates of organic export? Deep Sea Res. Part I Oceanogr. Res. Pap. 68, 24–45. doi:10.1016/j.dsr.2012.05.015

Rutgers van der Loeff, M.M., Buesseler, K.O., Bathmann, U., Hense, I., Andrews, J., 2002. Comparison of carbon and opal export rates between summer and spring bloom periods in the region of the Antarctic Polar Front, SE Atlantic. Deep Sea Res. Part II Top. Stud. Oceanogr. 49, 3849–3869. doi:10.1016/S0967-0645(02)00114-5

Rutgers van der Loeff, M.M., Cai, P., Stimac, I., Bracher, A., Middag, R., Klunder, M., Van Heuven, S., 2011. 234Th in surface waters: distribution of particle export flux across the Antarctic Circumpolar Current and in the Weddell Sea during the GEOTRACES expedition ZERO and DRAKE. Deep. Res. Part II Top. Stud. Oceanogr. 58, 2749–2766. doi:10.1016/j.dsr2.2011.02.004

Rutgers van der Loeff, M.M., Friedrich, J., Bathmann, U. V., 1997. Carbon export during the Spring Bloom at the Antarctic Polar Front, determined with the natural tracer 234Th. Deep Sea Res. Part II Top. Stud. Oceanogr. 44, 457–478. doi:10.1016/S0967-0645(96)00067-7

Rutgers van der Loeff, M.M., Sarin, M.M., Baskaran, M., Benitez-Nelson, C., Buesseler, K.O., Charette, M., Dai, M., Gustafsson, Ö., Masqué, P., Morris, P.J., Orlandini, K., Rodriguez y Baena, A., Savoye, N., Schmidt, S., Turnewitsch, R.,

931 Vöge, I., Waples, J.T., 2006. A review of present techniques and methodological
932 advances in analyzing 234Th in aquatic systems. Mar. Chem. 100, 190–212.
933 doi:10.1016/j.marchem.2005.10.012

934 Rutgers van der Loeff, M.M., Vöge, I., 2001. Does Fe fertilisation enhance the export
935 production as measured through the 234Th/238U disequilibrium in surface water?
936 In: The expeditions ANTARKTIS XVIII/1-2 of the research vessel "Polarstern" in
937 2000. Reports on Polar and Marine Research 400. Bremerhaven.

938 Salter, I., Lampitt, R.S., Sanders, R., Poulton, A., Kemp, A.E.S., Boorman, B., Saw, K.,
939 Pearce, R., 2007. Estimating carbon, silica and diatom export from a naturally
940 fertilised phytoplankton bloom in the Southern Ocean using PELAGRA: A novel
941 drifting sediment trap. Deep Sea Res. Part II Top. Stud. Oceanogr. 54, 2233–2259.
942 doi:10.1016/j.dsr2.2007.06.008

943 Savoye, N., Benitez-Nelson, C., Burd, A.B., Cochran, J.K., Charette, M., Buesseler,
944 K.O., Jackson, G.A., Roy-Barman, M., Schmidt, S., Elskens, M., 2006. 234Th
945 sorption and export models in the water column: A review. Mar. Chem. 100, 234–
946 249. doi:10.1016/j.marchem.2005.10.014

947 Savoye, N., Buesseler, K.O., Cardinal, D., Dehairs, F., 2004. 234Th deficit and excess
948 in the Southern Ocean during spring 2001: Particle export and remineralization.
949 Geophys. Res. Lett. 31, L12301. doi:10.1029/2004GL019744

950 Savoye, N., Trull, T.W., Jacquet, S.H.M., Navez, J., Dehairs, F., 2008. 234Th-based
951 export fluxes during a natural iron fertilization experiment in the Southern Ocean
952 (KEOPS). Deep Sea Res. Part II Top. Stud. Oceanogr. 55, 841–855.
953 doi:10.1016/j.dsr2.2007.12.036

954 Schlitzer, R., 2002. Carbon export fluxes in the Southern Ocean: results from inverse
955 modeling and comparison with satellite-based estimates. Deep Sea Res. Part II
956 Top. Stud. Oceanogr. 49, 1623–1644. doi:10.1016/S0967-0645(02)00004-8

957 Smetacek, V., 1999. Diatoms and the ocean carbon cycle. Protist 150, 25–32.
958 doi:10.1016/S1434-4610(99)70006-4

959 Smetacek, V., Klaas, C., Strass, V.H., Assmy, P., Montresor, M., Cisewski, B., Savoye,
960 N., Webb, A., D'Ovidio, F., Arrieta, J.M., Bathmann, U., Bellerby, R., Berg, G.M.,
961 Croot, P., Gonzalez, S., Henjes, J., Herndl, G.J., Hoffmann, L.J., Leach, H., Losch,
962 M., Mills, M.M., Neill, C., Peeken, I., Röttgers, R., Sachs, O., Sauter, E., Schmidt,
963 M.M., Schwarz, J., Terbrüggen, A., Wolf-Gladrow, D., 2012. Deep carbon export
964 from a Southern Ocean iron-fertilized diatom bloom. Nature 487, 313–9.
965 doi:10.1038/nature11229

966 Smith, D.C., Simon, M., Alldredge, A.L., Azam, F., 1992. Intense hydrolytic enzyme
967 activity on marine aggregates and implications for rapid particle dissolution.
968 Nature 359, 139–142. doi:10.1038/359139a0

969 Strass, V.H., Leach, H., Prandke, H., Donnelly, M., Bracher, A., Wolf-Gladrow, D., this
970 issue. The physical environmental conditions of biogeochemical differences along
971 the ACC in the Atlantic Sector during late austral summer 2012. Deep Sea Res. II.

972 Takahashi, T., Sutherland, S.C., Sweeney, C., Poisson, A., Metzl, N., Tilbrook, B.,
973 Bates, N., Wanninkhof, R., Feely, R.A., Sabine, C., Olafsson, J., Nojiri, Y., 2002.
974 Global sea–air CO2 flux based on climatological surface ocean pCO2, and
975 seasonal biological and temperature effects. Deep Sea Res. Part II Top. Stud.
976 Oceanogr. 49, 1601–1622. doi:10.1016/S0967-0645(02)00003-6

977 Turner, J.T., 2015. Zooplankton fecal pellets, marine snow, phytodetritus and the
978 ocean's biological pump. Prog. Oceanogr. 130, 205–248.
979 doi:10.1016/j.pocean.2014.08.005

980 Uitz, J., Claustre, H., Griffiths, F.B., Ras, J., Garcia, N., Sandroni, V., 2009. A
981 phytoplankton class-specific primary production model applied to the Kerguelen
982 Islands region (Southern Ocean). Deep. Res. I 56, 541–560.
983 doi:10.1016/j.dsr.2008.11.006

984 Usbeck, R., Rutgers van der Loeff, M.M., Hoppema, M., Schlitzer, R., 2002. Shallow
985 remineralization in the Weddell Gyre. Geochemistry Geophys. Geosystems 3, 1–
986 18. doi:10.1029/2001GC000182

987 Wolf-Gladrow, D., 2013. The Expedition of the Research Vessel "Polarstern" to the
988 Antarctic in 2012 (ANT-XXVIII/3). Reports on Polar and Marine Research 661.
989 Bremerhaven.

990 Wright, S.W., van den Enden, R.L., Pearce, I., Davidson, A.T., Scott, F.J., Westwood,
991 K.J., 2010. Phytoplankton community structure and stocks in the Southern Ocean
992 (30–80°E) determined by CHEMTAX analysis of HPLC pigment signatures. Deep
993 Sea Res. Part II Top. Stud. Oceanogr. 57, 758–778. doi:10.1016/j.dsr2.2009.06.015

994

995 Captions of Figures and Tables

996 Fig. 1: Study area and sampled stations for 234Th, POC and PON analyses. C
997 represents the central station, which was occupied 7 times: C91, C98, C99, C114, C128,
998 C136, C140. See Table 1 for further details regarding sampling dates. The satellite plot
999 represents the mean Chl-a concentration from the OC-CCI Chl-a product version-2
1000 during the sampling period (29 Jan. to 17 Feb. 2012).
1001
1002 Fig. 2: Vertical activity profiles for ^{234}Th (black diamonds) and ^{238}U (dotted line) from
1003 10 to 500-750 m depth. Grey shaded area indicates surface ^{234}Th deficits respect to ^{238}U.
1004 ^{238}U was derived from salinity (Owens et al., 2011). Primary Production Zone (PPZ,
1005 dashed grey line) is defined as the depth at which fluorescence reaches 10% of its
1006 maximum value (Owens, 2013).
1007
1008 Fig. 3: ^{234}Th export fluxes derived from seawater at 100 m (in white) and 300 m (in
1009 grey) assuming steady state conditions. The negligence of horizontal advection would
1010 lead to an error on these estimates of 580 ± 440 dpm m^{-2} d^{-1} at 100 m and 1500 ± 1700
1011 dpm m^{-2} d^{-1} at 300 m (i.e. ~25% and ~50%, respectively, see text for further details).
1012
1013 Fig. 4: POC vs Chl-a: (A) inventories in the upper 100 m of the water column, and (B)
1014 fluxes measured with sediment traps at 100 m (in white) and 300 m (in black).
1015
1016 Fig. 5: Pigment composition of sediment trap samples at 100 and 300 m. (A) Chl-a_{ST}
1017 fluxes, total pheopigment (TPheo) fluxes, and ratios of total pheopigment to Chl-a_{ST}
1018 fluxes (TPheo/Chl-a_{ST}); (B) fucoxanthin (Fuco), 19-hexanoyloxyfucoxanthin (19-Hex),
1019 and zeaxanthin (Zea) fluxes; (C) percentage of phytoplankton size classes:
1020 microphytoplankton (Micro), nanophytoplankton (Nano) and picophytoplankton (Pico).
1021
1022 Fig. 6: (A) POC export fluxes (F_C) at 100 m vs integrated net primary production (NPP)
1023 at 100 m, and (B) POC export fluxes at 300 m vs POC export fluxes at 100 m. Solid
1024 lines indicate the export and transfer efficiencies in (A) and (B), respectively. POC
1025 export fluxes were estimated using three methods: ST (diamonds), SWST (squares) and
1026 SWISP (circles, see text for further details).
1027
1028 Tab. 1: Location and date of the stations sampled for ^{234}Th, POC and PON analyses. C
1029 indicates the central station.
1030
1031 Tab. 2: Sampling of particles using sediment traps and *in-situ* pumps: location, depth,
1032 date, duration of the deployment (sediment traps) and filtered volume (*in-situ* pumps).
1033
1034 Tab. 3: ^{234}Th export fluxes derived from seawater ($F_{Th,SW}$) assuming steady state
1035 conditions, together with the fluxes derived directly from the sediment traps ($F_{Th,ST}$) at
1036 different depths.
1037
1038 Tab. 4: ^{234}Th export fluxes derived from seawater ($F_{Th,SW}$) at 100 and 300 m at the
1039 central station assuming non-steady state conditions. t_2-t_1 is the time interval between
1040 two occupations of the central station.
1041
1042 Tab. 5: POC/^{234}Th and PON/^{234}Th (C/Th and N/Th) ratios in particles collected using
1043 sediment traps (ST) and *in-situ* pumps (ISP, particles >53 μm), and POC and PON

export fluxes (F_C and F_N) estimated using the ST, SWST and SWISP methods at different depths (see text for further details).

*Calculated from the filter used for POC analysis. The filter used for ^{234}Th and POC analyses has not been considered because it was likely contaminated with organic carbon, presenting unusually high C/N molar ratio (14) compared with our overall sample average (8 ± 1).

Tab. 6: Export and transfer efficiencies using the POC export estimated from the ST, SWST and SWISP methods (see text for further details).

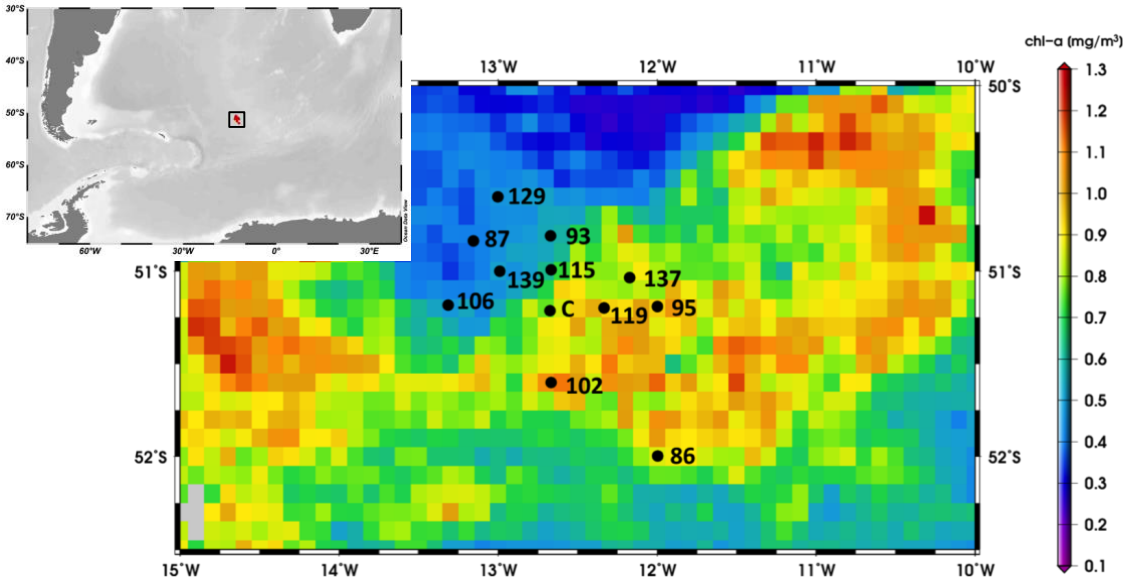

Fig. 1: Study area and sampled stations for ^{234}Th, POC and PON analyses. C represents the central station, which was occupied 7 times: C91, C98, C99, C114, C128, C136, C140. See Table 1 for further details regarding sampling dates. The satellite plot represents the mean Chl-a concentration from the OC-CCI Chl-a product version-2 during the sampling period (29 Jan. to 17 Feb. 2012).

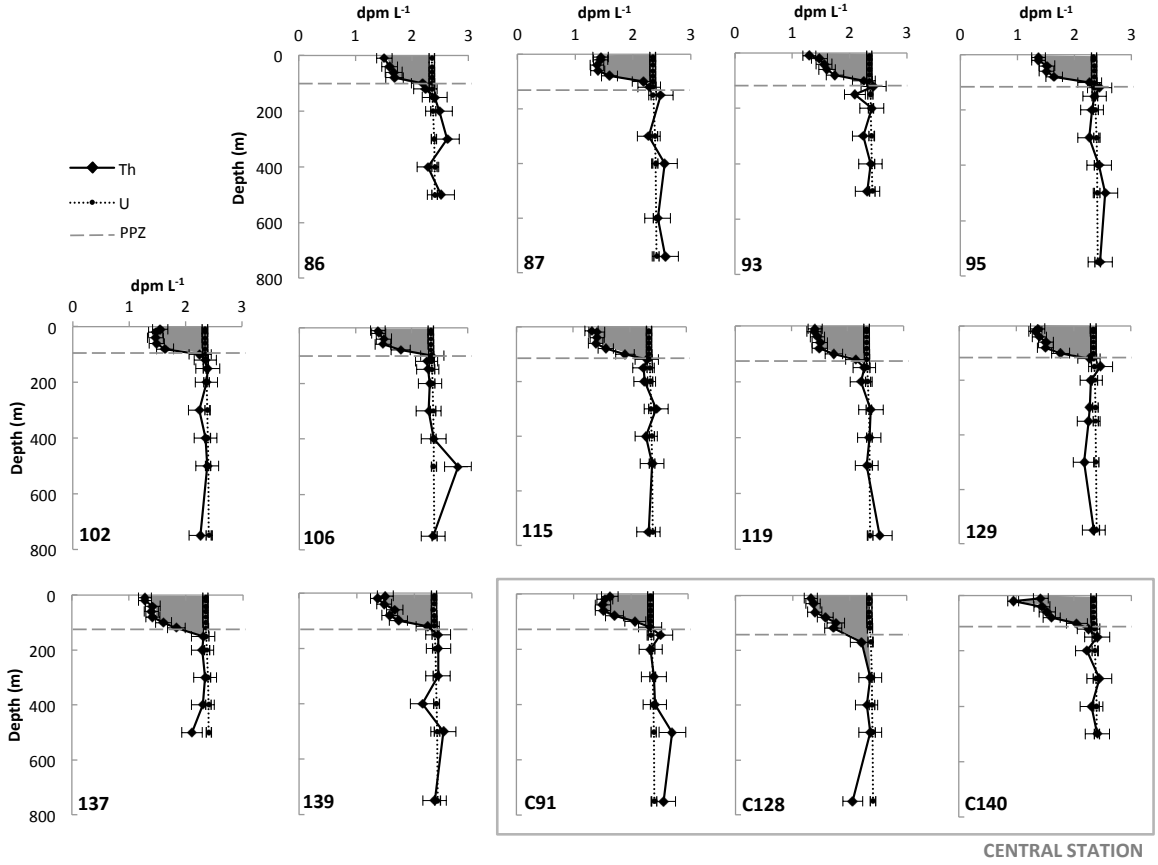

Fig. 2: Vertical activity profiles for ^{234}Th (black diamonds) and ^{238}U (dotted line) from 10 to 500-750 m depth. Grey shaded area indicates surface ^{234}Th deficits respect to ^{238}U. ^{238}U was derived from salinity (Owens et al., 2011). Primary Production Zone (PPZ, dashed grey line) is defined as the depth at which fluorescence reaches 10% of its maximum value (Owens, 2013).

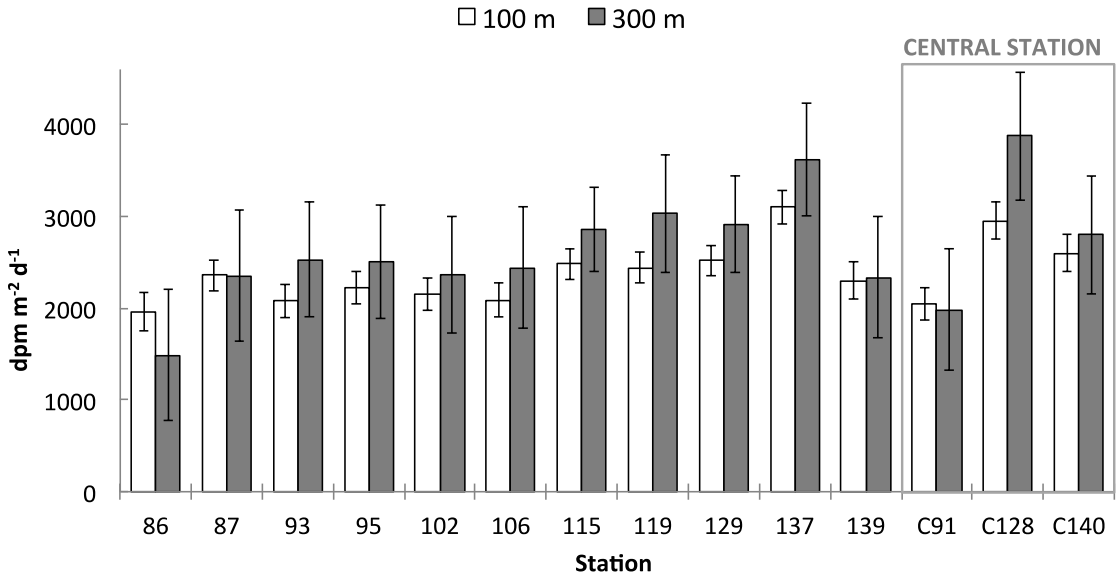

Fig. 3: ^{234}Th export fluxes derived from seawater at 100 m (in white) and 300 m (in grey) assuming steady state conditions. The negligence of horizontal advection would lead to an error on these estimates of 580 ± 440 dpm m^{-2} d^{-1} at 100 m and 1500 ± 1700 dpm m^{-2} d^{-1} at 300 m (i.e. ~25% and ~50%, respectively, see text for further details).

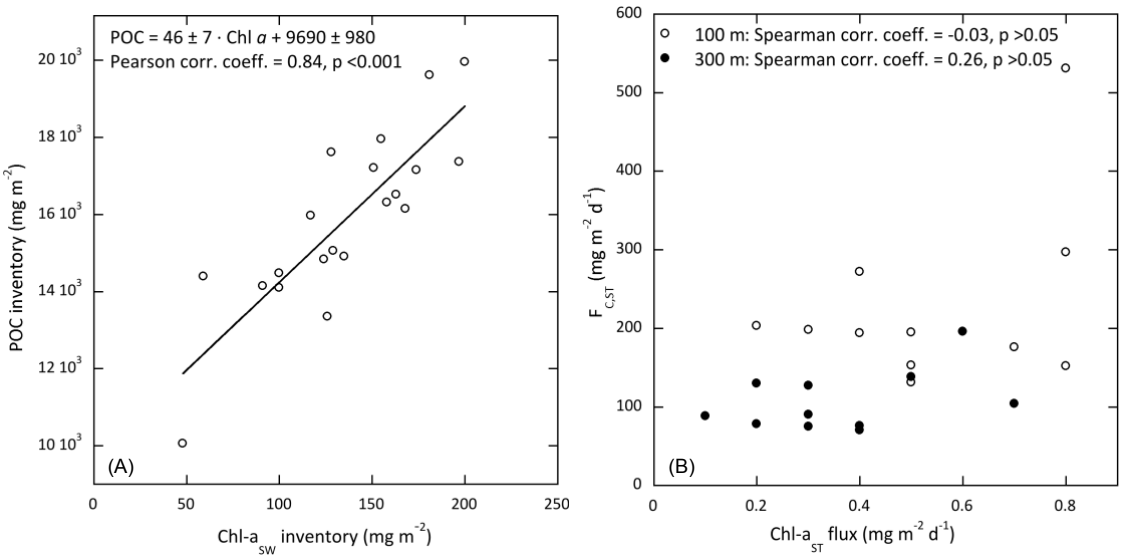

Fig. 4: POC vs Chl-a: (A) inventories in the upper 100 m of the water column, and (B) fluxes measured with sediment traps at 100 m (in white) and 300 m (in black).

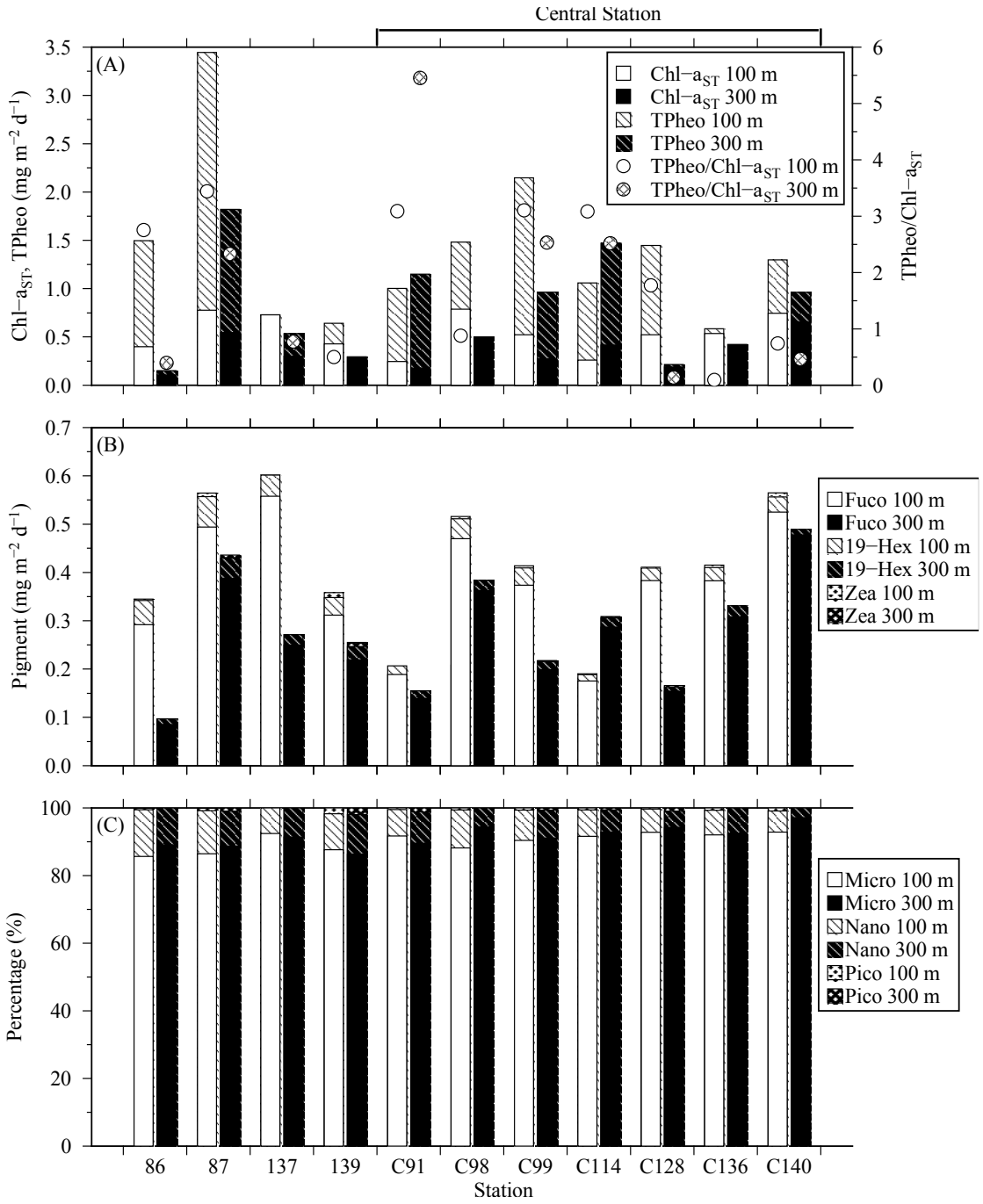

Fig. 5: Pigment composition of sediment trap samples at 100 and 300 m. (A) Chl-a$_{ST}$ fluxes, total pheopigment (TPheo) fluxes, and ratios of total pheopigment to Chl-a$_{ST}$ fluxes (TPheo/Chl-a$_{ST}$); (B) fucoxanthin (Fuco), 19-hexanoyloxyfucoxanthin (19-Hex), and zeaxanthin (Zea) fluxes; (C) percentage of phytoplankton size classes: microphytoplankton (Micro), nanophytoplankton (Nano) and picophytoplankton (Pico).

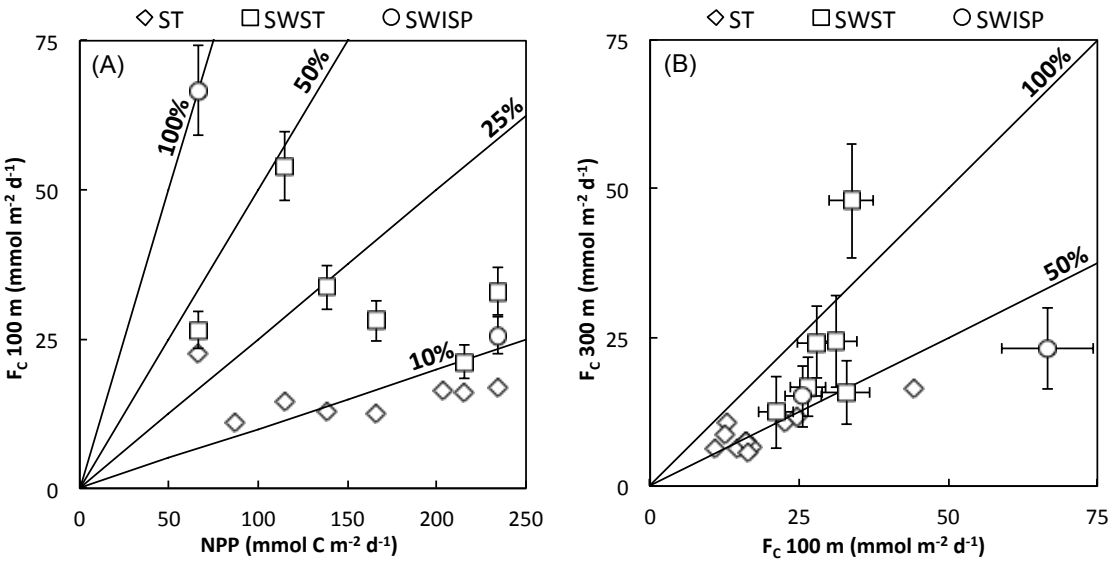

Fig. 6: (A) POC export fluxes (F_C) at 100 m vs integrated net primary production (NPP) at 100 m, and (B) POC export fluxes at 300 m vs POC export fluxes at 100 m. Solid lines indicate the export and transfer efficiencies in (A) and (B), respectively. POC export fluxes were estimated using three methods: ST (diamonds), SWST (squares) and SWISP (circles, see text for further details).

Tab. 1: Location and date of the stations sampled for ^{234}Th, POC and PON analyses. C indicates the central station.

Station	Lon. (ºW)	Lat. (ºS)	Date (2012)
86	12.00	52.00	29-30 Jan.
87	13.16	50.84	2-3 Feb.
93	12.67	50.81	4 Feb.
95	12.00	51.19	5 Feb.
102	12.67	51.60	7 Feb.
106	13.31	51.18	7 Feb.
115	12.67	50.99	9 Feb.
119	12.33	51.20	10 Feb.
129	13.00	50.60	13 Feb.
137	12.17	51.04	14-15 Feb.
139	12.99	51.00	15-16 Feb.
C91	12.67	51.21	3-5 Feb.
C98	12.67	51.21	5-6 Feb.
C99	12.67	51.21	6-8 Feb.
C114	12.67	51.21	8-11 Feb.
C128	12.67	51.21	12-13 Feb.
C136	12.67	51.21	14-15 Feb.
C140	12.67	51.21	16-17 Feb.

Tab. 2: Sampling of particles using sediment traps and *in-situ* pumps: location, depth, date, duration of the deployment (sediment traps) and filtered volume (*in-situ* pumps).

Station	Lon. (ºW)	Lat. (ºS)	Deployment sediment traps			Deployment *in-situ* pumps		
			Depth (m)	Date (2012)	Duration (h)	Depth (m)	Date (2012)	Volume (L)
86	12.00	52.00	100, 300	29 Jan.	23			
87	13.16	50.84	100, 300	2 Feb.	20			
137	12.17	51.04	120, 320	14 Feb.	15			
139	12.99	51.00	120, 320	15 Feb.	19	100, 150, 300, 400	16 Feb.	250-900
C91	12.67	51.21	100, 300	3 Feb.	53	100, 150, 300, 400	3 Feb.	450-1200
C98	12.67	51.21	100, 300	5 Feb.	18			
C99	12.67	51.21	100, 300	6 Feb.	50			
C114	12.67	51.21	100, 300	8 Feb.	72			
C128	12.67	51.21	120, 320	12 Feb.	29			
C136	12.67	51.21	120, 320	14 Feb.	22			
C140	12.67	51.21	120, 320	16 Feb.	18			

Tab. 3: ^{234}Th export fluxes derived from seawater ($F_{Th,SW}$) assuming steady state conditions, together with the fluxes derived directly from the sediment traps ($F_{Th,ST}$) at different depths.

Station	Depth (m)	$F_{Th,SW}$ (dpm m^{-2} d^{-1})	$F_{Th,ST}$ (dpm m^{-2} d^{-1})
86	100	1960 ± 210	1700 ± 140
	300	1490 ± 710	970 ± 80
87	100	2360 ± 170	4000 ± 320
	300	2350 ± 710	1990 ± 170
93	100	2080 ± 180	
	300	2530 ± 630	
95	100	2220 ± 180	
	300	2510 ± 620	
102	100	2150 ± 180	
	300	2360 ± 640	
106	100	2090 ± 190	
	300	2440 ± 660	
115	100	2480 ± 170	
	300	2860 ± 470	
119	100	2440 ± 170	
	300	3020 ± 640	
129	100	2520 ± 170	
	300	2910 ± 520	
137	120	3100 ± 180	1090 ± 100
	300-320	3620 ± 620	620 ± 60
139	120	2510 ± 200	2440 ± 200
	150	2540 ± 260	
	300-320	2340 ± 660	1870 ± 160
	400	2660 ± 900	
C91	100	2050 ± 180	1470 ± 120
	150	2070 ± 270	
	300	1980 ± 660	900 ± 70
	400	1910 ± 910	
C98	100		1430 ± 120
	300		790 ± 70
C99	100		1370 ± 110
	300		960 ± 80
C114	100		1200 ± 100
	300		590 ± 50
C128	120	2950 ± 200	1050 ± 90
	300-320	3870 ± 700	920 ± 80
C140	120	2600 ± 210	1450 ± 130
	300-320	2800 ± 650	1220 ± 110

Tab. 4: ^{234}Th export fluxes derived from seawater ($F_{Th,SW}$) at 100 and 300 m at the central station assuming non-steady state conditions. t_2-t_1 is the time interval between two occupations of the central station.

Stations	t_2-t_1 (days)	Depth (m)	$F_{Th,SW}$ (dpm m^{-2} d^{-1})
C91-C128	10	100	4290 ± 880
		300	9600 ± 3400
C128-C140	4	100	1600 ± 2000
		300	-5500 ± 7600

Tab. 5: POC/^{234}Th and PON/^{234}Th (C/Th and N/Th) ratios in particles collected using sediment traps (ST) and *in-situ* pumps (ISP, particles >53 μm), and POC and PON export fluxes (F_C and F_N) estimated using the ST, SWST and SWISP methods at different depths (see text for further details).

Station	Depth (m)	C/Th (μmol dpm^{-1})		N/Th (μmol dpm^{-1})		F_C (mmol m^{-2} d^{-1})			F_N (mmol m^{-2} d^{-1})		
		ST	ISP (> 53 μm)	ST	ISP (> 53 μm)	ST	SWST	SWISP	ST	SWST	SWISP
86	100	10.8 ± 0.9		1.4 ± 0.1		16	21 ± 3		2.0	2.6 ± 0.4	
	300	8.3 ± 0.7		0.85 ± 0.07		7.3	12 ± 6		0.74	1.3 ± 0.6	
87	100	13 ± 1		1.5 ± 0.1		44	31 ± 3		5.1	3.6 ± 0.4	
	300	10.3 ± 0.9		1.05 ± 0.09		16	24 ± 8		1.7	2.5 ± 0.8	
137	120	17 ± 2		2.2 ± 0.2		15	54 ± 6		1.8	6.7 ± 0.7	
	320					*6.3					
139	100-120	10.6 ± 0.9	29 ± 2	1.2 ± 0.1	5.2 ± 0.4	23	26 ± 3	67 ± 8	2.5	2.9 ± 0.3	12 ± 1
	150		20 ± 2		2.8 ± 0.3			52 ± 7			7 ± 1
	300-320	7.1 ± 0.6	9.9 ± 0.9	0.89 ± 0.07	1.1 ± 0.1	11	17 ± 5	23 ± 7	1.3	2.1 ± 0.6	2.6 ± 0.8
	400		9.0 ± 0.8		1.3 ± 0.1			24 ± 8			3 ± 1
C91	100	16 ± 1	13 ± 1	1.9 ± 0.2	2.1 ± 0.2	17	33 ± 4	26 ± 3	2.0	4.0 ± 0.5	4.2 ± 0.5
	150		12 ± 1		1.7 ± 0.1			25 ± 4			3.5 ± 0.5
	300	7.9 ± 0.6	7.6 ± 0.6	0.90 ± 0.07	1.3 ± 0.1	6.5	16 ± 5	15 ± 5	0.74	1.8 ± 0.6	2.5 ± 0.9
	400		4.3 ± 0.3		0.73 ± 0.06			8 ± 4			1.4 ± 0.7
C98	100	19 ± 2		2.4 ± 0.2		25			3.1		
	300	17 ± 2		1.8 ± 0.2		12			1.2		
C99	100	15 ± 1		1.8 ± 0.1		16			2.0		
	300	9.1 ± 0.8		1.06 ± 0.09		7.5			0.88		
C114	100	14 ± 1		1.9 ± 0.2		16			2.3		
	300	9.8 ± 0.8		1.3 ± 0.1		5.8			0.77		
C128	120	11 ± 1		1.6 ± 0.1		13	34 ± 4		1.7	4.6 ± 0.5	
	320	12 ± 1		1.1 ± 0.1		11	50 ± 10		1.0	4.3 ± 0.9	
C136	120					11					
	320					6.3					
C140	120	11 ± 1		1.3 ± 0.1		13	28 ± 3		1.6	3.5 ± 0.4	
	320	8.6 ± 0.8		1.1 ± 0.1		8.6	24 ± 6		1.1	3.0 ± 0.8	

*Calculated from the filter used for POC analysis. The filter used for ^{234}Th and POC analyses has not been considered because it was likely contaminated with organic carbon, presenting unusually high C/N molar ratio (14) compared with our overall sample average (8 ± 1).

Tab. 6: Export and transfer efficiencies using the POC export estimated from the ST, SWST and SWISP methods (see text for further details).

Station	Export efficiency (%)			Transfer efficiency (%)		
	ST	SWST	SWISP	ST	SWST	SWISP
86	7.5	10 ± 1		45	60 ± 30	
87				37	80 ± 30	
137	13	47 ± 5		43		
139	34	40 ± 5	100 ± 10	47	60 ± 20	30 ± 10
C91	7.2	14 ± 2	11 ± 1	38	50 ± 20	60 ± 20
C98				47		
C99				46		
C114	8.1			35		
C128	9.2	24 ± 3		84	140 ± 30	
C136	12			58		
C140	7.6	17 ± 2		68	90 ± 20	